26

Superconductivity

As discussed in Chapter 24, the electrical resistivity of metals decreases with decreasing temperature. In spite of zero-point vibrations, the contribution of scattering by lattice vibrations would vanish at $T = 0$, and the resistivity of an ideal crystal would be zero, whereas finite resistivities would be observed at any finite temperature. However, impurities and inhomogeneities, which are always present in the sample, reduce the transport relaxation time of electrons to a finite value even at zero temperature, and thus the conductivity remains finite at $T = 0$, too: $\sigma = n_e e^2 \tau / m_e$ according to the prediction of the Drude model. The liquefaction of helium (1908) opened the way to studying the resistivity of metals at much lower temperatures than before, well below the condensation point of helium at 4.22 K, also known as the liquid-helium temperature. It came as a great surprise in 1911 when H. Kamerlingh Onnes[1] observed that the resistivity of mercury (which can be purified easily in its liquid state, and is therefore regarded as the purest metal) did not decrease gradually with decreasing temperature but dropped to a very low value – zero within experimental error – around $T = 4.2$ K. This experimental finding is shown in Fig. 26.1.

Later it was confirmed that in a broad class of metals the resistivity does not decrease gradually, as a power of the temperature, but drops suddenly to zero at a finite critical temperature T_c. Kamerlingh Onnes coined the terms *superconductor* for such materials, and *superconductivity* for the phenomenon.[2]

In most cases the superconducting state appears at a very low temperature, however several families of materials have been discovered recently in which the transition temperature is close to or even somewhat higher than 100 K. Depending on the purity of the sample, the transition may be slightly smeared out, as in the example shown in Fig. 26.2. The resistance of the sample of

[1] See the footnote on page 2 of Volume 1.

[2] Originally, he dubbed the phenomenon "supraconductivity", but this name was gradually replaced by the term used today.

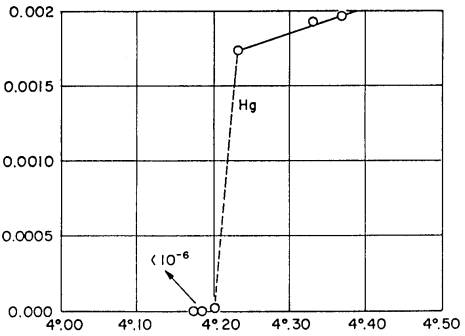

Fig. 26.1. Temperature dependence of the resistivity of mercury at low temperatures, as measured by KAMERLINGH ONNES [*Comm. Phys. Lab. Univ. Leiden*, No. 120b (1911)]

composition $YBa_2Cu_3O_{7-\delta}$ (abbreviated as Y-Ba-Cu-O or YBCO) starts to decrease rapidly around 90 K, but it is finite even at 80 K.

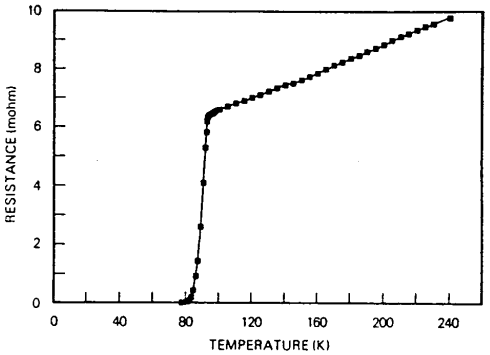

Fig. 26.2. Temperature dependence of the resistance for a high-T_c superconductor, Y-Ba-Cu-O [Reprinted with permission from M. K. Wu et al., *Phys. Rev. Lett.* **58**, 908 (1987). ©1987 by the American Physical Society]

We shall start this chapter with a brief overview of the phenomenon of superconductivity and the most characteristic properties of superconductors, and then give a phenomenological description. The microscopic theory will be presented in Chapter 34 (Volume 3), after the detailed discussion of electron–electron interactions.

26.1 Superconductivity: The Phenomenon

Even though the most striking feature of superconductors is their infinitely high conductivity, it is accompanied by a number of other interesting properties. Their discovery was a great step toward the understanding of the phenomenon. Below we shall consider them one by one.

26.1.1 Vanishing Resistance, Persistent Current

The name "superconductor" comes from the striking property of vanishing resistance below a critical temperature. A direct consequence of this vanishing resistance is the persistence of currents. In a ring-shaped superconductor a current would flow indefinitely because of the absence of resistance. According to experiments, there is no sign indicating that the current would diminish: the most precise measurements put the lifetime of the current above 10^5 years. As we shall see, this current flows on the sample surface and not in its interior.

However, superconductors cannot carry arbitrarily large currents. Above a critical current J_c the sample ceases to behave as a superconductor. In wires of 1 mm in diameter this critical current can be as high as 100 A. As we shall see, it is the magnetic field, generated by the current around the sample, that destroys superconductivity.

The statement that no current is dissipated is valid only for direct currents and low-frequency alternating currents. Current is dissipated above a threshold frequency ν, which is characteristic of the material and is usually in the microwave or infrared region. This can be seen in Fig. 26.3, which shows the frequency dependence of the real part of the optical conductivity in thin lead layers. It can be shown that the threshold frequency and the width Δ of the

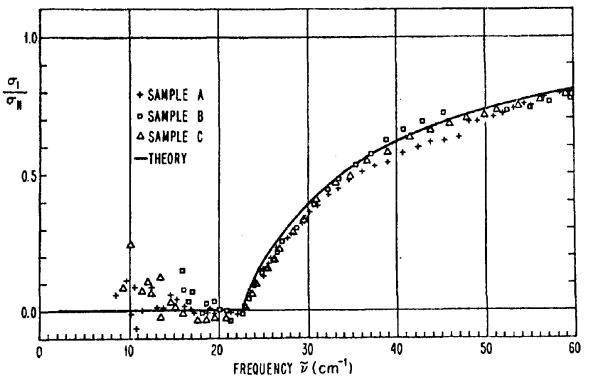

Fig. 26.3. The frequency dependence of the real part of the optical (far-infrared) conductivity in thin lead layers [Reprinted with permission from L. H. Palmer and M. Tinkham, *Phys. Rev.* **165**, 588 (1968). ©1968 by the American Physical Society]

gap in the energy spectrum (to be discussed in Section 26.1.6) are related by $h\nu \approx \Delta$.

26.1.2 Isotope Effect

In 1950 several research groups observed that the critical temperature T_c of superconductors depended on the isotopic composition: T_c was found to decrease for increasing concentrations of heavier isotopes of the same element. For mercury, which has seven stable isotopes between mass numbers 196 and 204, the transition temperature varies between 4.16 K and 4.12 K. The dependence of the critical temperature on the isotopic mass can be approximated as

$$T_c \propto M^{-\alpha}\,, \tag{26.1.1}$$

where $\alpha = 1/2$ was found for mercury. In other cases the variations of the critical temperature are weaker. Table 26.1 shows the measured value of α for a number of superconductors.

Table 26.1. Measured value of exponent α of the isotope effect for a number of superconductors

	Cd	Hg	Mo	Os	Pb	Re	Ru	Sn	Tl	Zn	Zr
α	0.5	0.50	0.37	0.21	0.48	0.36	0.0	0.47	0.5	0.45	0.0

While in certain cases the exponent is zero – which corresponds to the absence of any measurable isotope effect –, it is often close to 0.5. Since different isotopes have the same electronic structure, the dependence on the isotopic composition indicates that superconductivity cannot be understood completely in terms of the electron system alone: the mass of the ions in whose field the electrons move is also important. As we shall see in Chapter 34, the microscopic theory of superconductivity – the BCS theory – provides a simple explanation for the dependence on the isotopic mass and the exponent $\alpha = 1/2$. Deviations from it can be understood in an improved theoretical framework that leads to the Eliashberg equations.

26.1.3 Meissner–Ochsenfeld Effect

Because of its infinite conductivity, the superconductor might be considered as a perfect conductor. In perfect conductors the current flow can be finite only for vanishing electric fields, $\boldsymbol{E} = 0$. However, the Maxwell equations then imply that the magnetic field cannot vary with time inside the sample. Therefore, when an external magnetic field is turned on, it cannot penetrate

into the perfectly conducting region. On the other hand, if the sample is placed in a magnetic field in its normal state, and it becomes a perfect conductor only afterwards, then the magnetic field established inside the sample in the normal state would need to remain unaltered by the transition into the perfect conductor state, and the magnetic field would freeze into the sample. This means that the strength of the magnetic field in a perfect conductor would depend on the history of the sample.

Contrary to these expectations, W. Meissner and R. Ochsenfeld (1933) observed that the magnetic induction inside the superconductor was always zero in weak applied fields. When a superconductor is placed in a magnetic field, the field cannot penetrate into the sample. And if the sample is placed into the magnetic field in its normal state, and cooled below the critical temperature T_c only afterwards, the magnetic field is expelled from the sample. This is the *Meissner–Ochsenfeld effect*. The magnetic field lines are shown in Fig. 26.4 for both the normal and superconducting states.

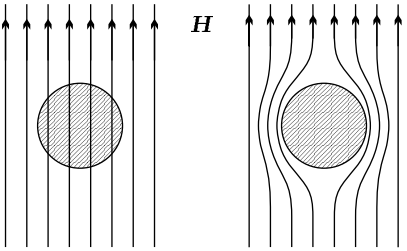

Fig. 26.4. The magnetic field lines around a sample of finite size, in the normal (left) and superconducting (right) states

To understand this behavior of superconductors, we have to assume that the magnetic field induces surface currents in a layer that is macroscopically thin but thick on the atomic scales. These cancel the applied field, and maintain the state in which the magnetic induction is zero inside the sample. In conjunction with the formula $\boldsymbol{B} = \mu_0(\boldsymbol{H} + \boldsymbol{M}) = 0$, the requirement $\boldsymbol{B} = 0$ leads to

$$\boldsymbol{M} = -\boldsymbol{H} \tag{26.1.2}$$

for the magnetization of the superconductor. The susceptibility of the superconductor is therefore $\chi_m = -1$, which corresponds to perfect diamagnetism.

This property of superconductors can be exploited most easily for setting up a persistent current. Consider a superconducting ring placed in a uniform axial magnetic field $\boldsymbol{H}$ above its critical temperature. With the field switched on, the sample is then cooled below its critical temperature, whereby the magnetic field $\boldsymbol{H}$ is expelled from the sample but, of course, $\boldsymbol{B}$ remains finite inside the ring. When the external field is then switched off, the field strength inside the ring must remain unchanged, since field lines cannot enter the

superconducting ring. Therefore the flux through the ring is the same as the original flux of the applied field: the transient electric field generated by the switch-off induces an eddy current in the ring, and the magnetic field of the current produces the required flux. The magnetic field lines around the ring in the presence of the applied field and after its switch-off are shown in Fig. 26.5.

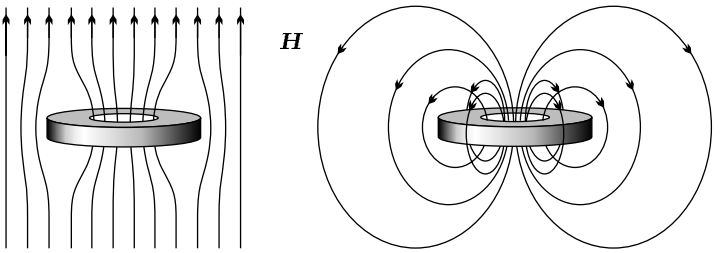

Fig. 26.5. The magnetic field lines around a ring-shaped sample in the presence of an applied field (left) and after the applied field has been switched off (right), when the superconducting current induced in the sample maintains the flux through the ring

According to the measurement results shown in Fig. 26.6, the flux through the superconducting ring cannot take any arbitrary value, only the integral multiples of the flux quantum $\Phi_0 = h/2e$. This flux quantum is exactly the half of what would be expected from the Landau quantization of electronic energy levels in strong magnetic fields.[3]

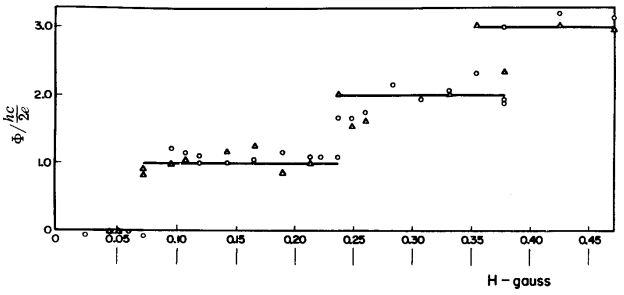

Fig. 26.6. The magnetic flux through a superconducting ring, as a function of the applied field [Reprinted with permission from B. S. Deaver, Jr. and W. M. Fairbank, *Phys. Rev. Lett.* **7**, 43 (1961). ©1961 by the American Physical Society]

[3] The flux quantum associated with the motion of electrons in a magnetic field is h/e, see page 282.

26.1.4 Critical Field

The Meissner–Ochsenfeld effect can usually be observed only in relatively weak fields. Sufficiently strong fields – which may be as low as $H \sim 10^2$ to 10^3 Oe in certain materials – can completely destroy superconductivity; the sample then shows normal metallic behavior. Depending on how the transition to the normal phase occurs, superconductors are divided into two broad classes.

In *type I superconductors* $\boldsymbol{B}$ remains zero inside the sample until the applied magnetic field reaches a temperature-dependent critical value $H_c(T)$; at that point the entire sample becomes normal, that is, its conductivity jumps to a finite value. As we shall see later, the transition is first order everywhere except $T = 0$ and at $T = T_c$ where $H_c = 0$, therefore the magnetization curve exhibits hysteresis. When the external magnetic field is reduced, the normal state may be maintained down to a lower field strength H_{c2} ($H_{c2} < H_c$). The magnetic induction inside the sample and the magnetization of the sample are shown in Fig. 26.7.

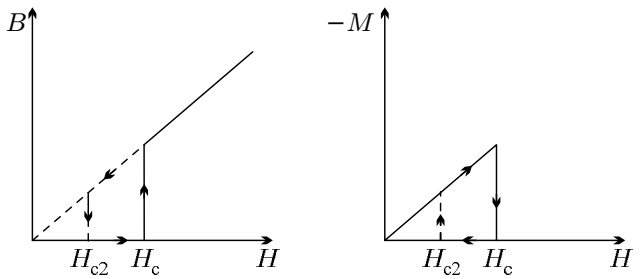

Fig. 26.7. The magnetic induction and magnetization in type I superconductors as functions of the applied magnetic field

Of course, at the critical temperature T_c the critical field is zero: $H_c(T_c) = 0$. At lower temperatures H_c is finite, and increases continuously as T decreases. Experimental data show that this dependence is well approximated by the function

$$H_c(T) = H_c(0)\left[1 - (T/T_c)^2\right]. \tag{26.1.3}$$

The critical field at $T = 0$ and the critical temperature are two important parameters of superconductors. The superconducting phase covers a finite region in the T–H plane; its boundary is determined by the temperature dependence of the critical field. A typical phase diagram is shown in Fig. 26.8.

However, this behavior is not common to all superconductors. In a fairly large proportion of superconductors the magnetic field starts to penetrate into the sample at the *lower critical field* H_{c1}, however this penetration is gradual rather than abrupt. The complete penetration of the field occurs at the *upper critical field* H_{c2}, where superconductivity is destroyed. Materials that

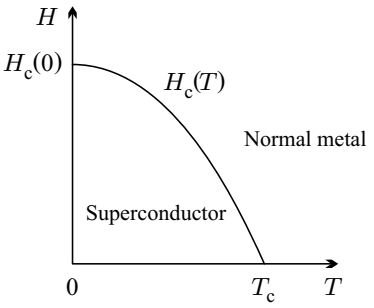

Fig. 26.8. Phase diagram of type I superconductors in the T–H plane

exhibit this behavior are called *type II superconductors*. The dependence of the magnetization and average magnetic flux density B in such superconductors on the applied magnetic field H are shown in Fig. 26.9.

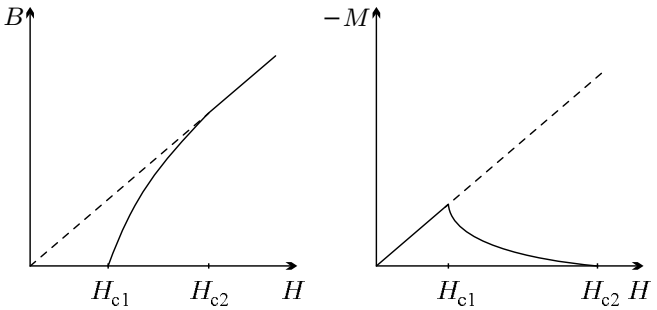

Fig. 26.9. The magnetic induction and the magnetization in type II superconductors as functions of the applied magnetic field

As opposed to type I superconductors, the penetration of the magnetic field (the disappearance of the Meissner–Ochsenfeld effect) in type II superconductors occurs at a lower field than the appearance of electrical resistivity. That is why there are two phase boundaries in the schematic phase diagram in Fig. 26.10.

When the applied field is weaker than the lower critical field H_{c1}, the sample behaves as a perfect diamagnet. This is the *Meissner phase*. When the applied field is stronger than the upper critical field H_{c2}, normal behavior is observed. For fields between H_{c1} and H_{c2}, in the *Shubnikov phase*, the sample becomes inhomogeneous: the sample interior then contains alternate superconducting and normal regions. That is why this phase is also known as the *mixed phase*. The normal phase appears inside tube-like regions ("filaments of flux") along the applied magnetic field; the magnetic field can penetrate into these parts of the sample. The magnetic flux density inside each tube is such

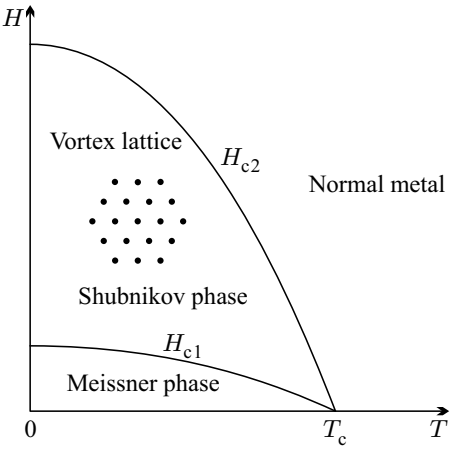

Fig. 26.10. Phase diagram of type II superconductors in the T–H plane

that the total magnetic flux through the tube is exactly one flux quantum. The current around the tube surface screens this flux, and the regions among the tubes are superconducting. Since these eddy currents show a vortex-like pattern, the tubes are called *vortices*. Defects in the crystalline order prevent the vortices from moving, and so externally applied currents may flow without any resistance in this state of the sample, too. Since H_{c2} may be as high as 10^5 Oe, type II superconductors are much more important for technological applications than type I superconductors. Among others, strong superconducting magnets can be built of them.

As we shall see, in conventional type II superconductors vortices are arranged in a regular array over the entire range between H_{c1} and H_{c2}. All high-T_c superconductors are type II materials, however their phase diagram is even more complicated, as the lattice of vortices may melt before the sample becomes a normal metal. Such a phase diagram is shown in Fig. 26.25.

26.1.5 Thermoelectric Properties

According to the Wiedemann–Franz law, good conductors are also good heat conductors. In the region where the electrical resistivity receives its dominant contribution from phonon-absorption and -emission processes, the resistivity increases with temperature, while the thermal conductivity decreases for a while and then tends to a constant value. The same behavior is observed in superconducting materials in their normal phase when a magnetic field exceeding H_c is applied. If the Wiedemann–Franz law were valid in the superconducting phase, too, then the thermal conductivity would also become infinitely large. However, λ starts to decrease at the onset of superconductivity, as shown in Fig. 26.11.

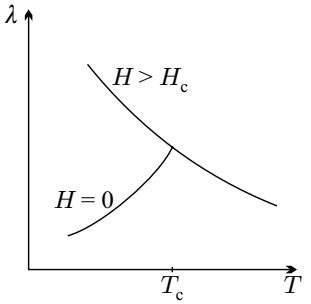

Fig. 26.11. Temperature dependence of the thermal conductivity in the vicinity of the superconducting phase transition

Another surprise is that the electric current is not accompanied by a heat current: the Peltier coefficient is zero in the superconducting phase. These phenomena indicate that the electrons responsible for superconductivity do not carry any entropy.

26.1.6 Specific Heat

As we have seen, below room temperature, the specific heat of pure metals in their normal state can be given as the sum of two terms:

$$C_{\mathrm{n}} = \gamma T + AT^3 \,. \tag{26.1.4}$$

The linear term, which becomes dominant at low temperatures, is the electronic contribution, while the cubic term is due to phonons. A completely different behavior is observed in the superconducting phase. The specific heat has a discontinuity at T_{c}, and immediately below T_{c} it is larger than it would be in the normal phase. On the other hand, the electronic contribution to the specific heat is exponentially small at low temperatures,

$$C_{\mathrm{s}} \sim \exp\left(-\frac{\Delta}{k_{\mathrm{B}}T}\right) , \tag{26.1.5}$$

where Δ is on the order of $k_{\mathrm{B}}T_{\mathrm{c}}$. This is shown for aluminum in Fig. 26.12.

This behavior indicates that, contrary to normal metals, there are no low-energy electronic excitations in the superconducting state. A gap $\Delta \sim k_{\mathrm{B}}T_{\mathrm{c}}$ appears in the excitation spectrum. However, this gap is different in several respects from those in semiconductors or insulators. Firstly, the appearance of the gap in the latter types of material is the consequence of the periodic potential of the lattice. When electrons are added to the system, they occupy states above the gap, and thus the conductivity increases. In contrast, the energy gap is attached to the Fermi energy in superconductors. If the number of electrons were increased, the position of the gap would be shifted upward together

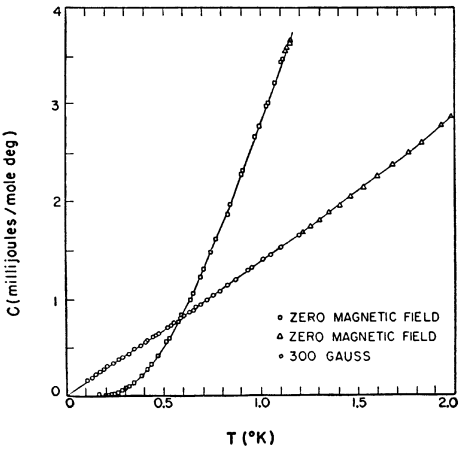

Fig. 26.12. Low-temperature specific heat of aluminum in zero magnetic field and in an external field exceeding H_c [Reprinted with permission from N. E. Phillips, *Phys. Rev.* **114**, 676 (1959). ©1959 by the American Physical Society]

with the chemical potential, and the system would remain a superconductor. Secondly, the gap depends only weakly on temperature in semiconductors, whereas it shows a strong temperature dependence in superconductors. The gap becomes narrower for increasing temperatures, and disappears at T_c.

In the absence of a magnetic field the superconducting order breaks up continuously: the phase transition is second order. However, the specific heat exhibits a discontinuity. Its magnitude can be estimated using the microscopic theory. Referred to the specific heat $C_n = \gamma T_c$ of the electron system, the relative jump of the specific heat is a universal constant:

$$\frac{C_s - C_n}{C_n} = \frac{12}{7\zeta(3)} = 1.426\,. \tag{26.1.6}$$

As can be seen in Table 26.2, the measured value is indeed close to this number in certain materials. However, the deviation is significant in others, especially in high-T_c superconductors, where the specific-heat contribution of phonons is also important.

Table 26.2. The relative jump of the specific heat in the transition point for some superconductors

Element	Relative jump	Compound	Relative jump
Al	1.45	UPt_3	0.9
Cd	1.36	$CeRu_2Si_2$	3.5
Nb	1.93	$(TMTSF)_2ClO_4$	1.7
Pb	2.71	$YBa_2Cu_3O_7$	3.6

Using the relation between the specific heat in a uniform magnetic field and the entropy per unit volume,

$$c_H = T \left(\frac{\partial s}{\partial T} \right)_H , \tag{26.1.7}$$

the entropy can be determined. Its temperature dependence is sketched in Fig. 26.13. The entropy is lower in the superconducting phase than it would be in the normal phase. The former is therefore more ordered than the latter.

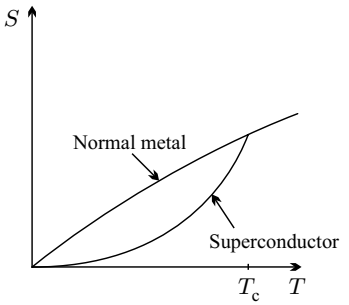

Fig. 26.13. Temperature dependence of the entropy in the superconducting and normal states

26.1.7 Tunneling in SIS and SIN Junctions

Other measurements also indicate the presence of a gap in the spectrum of electronic excitations. When a thin superconducting layer is illuminated by infrared radiation with a wavelength of a few mm ($E_{\text{photon}} \sim 10^{-3}\,\text{eV}$), absorption is observed only above a frequency threshold. The same applies to the absorption of ultrasound. As pointed out by I. Giaever[4] (1960), the experimental study of tunneling in junctions where two superconductors or a superconductor and a normal metal are separated by a thin insulator layer is likely to provide the most suitable method for detecting the energy gap in the superconducting phase. The first configuration is called a superconductor–insulator–superconductor (SIS) junction, and the second is a superconductor–insulator–normal metal (SIN) junction. The current–voltage characteristics of two SIS junctions are shown in Fig. 26.14. In the first case identical, and in the second case different superconducting materials are used on the two sides. In the I–V curve extrapolated to $T = 0$ the current appears only at a finite voltage, which is related to the energy gaps Δ_{L} and Δ_{R} of the superconductors on the left and right by $eV = \Delta_{\text{L}} + \Delta_{\text{R}}$.

[4] Ivar Giaever (1929–) was awarded the Nobel Prize in 1973 for his "experimental discoveries regarding tunneling phenomena in superconductors".

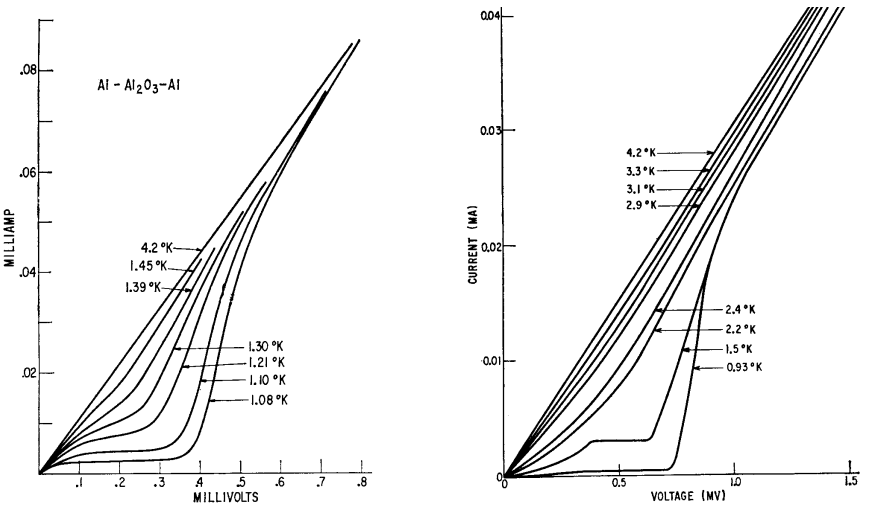

Fig. 26.14. Current–voltage characteristics of Al-Al_2O_3-Al and Al-Al_2O_3-In junctions at different temperatures [Reprinted with permission from I. Giaever and K. Megerle, *Phys. Rev.* **122**, 1101 (1961). ©1961 by the American Physical Society]

In junctions that contain high-T_c unconventional superconductors different characteristics and temperature dependence are observed. This is related to the characteristic anisotropy of the energy spectrum in such materials: the gap depends on the direction in $\boldsymbol{k}$-space.

26.2 Superconducting Materials

The first superconducting materials were discovered among elemental metals. Somewhat later, researchers turned to metallic compounds, and observed that quite a few of them became superconductors at low temperatures. By low temperatures we mean that even though the highest observed critical temperature kept growing, the record was still only 23 K in the mid-1980s. Shortly afterwards, high-T_c superconductors were discovered, with critical temperatures above 100 K. Nonetheless we are still very far from realizing the hope of finding materials that superconduct even at room temperature.

Below, we shall first consider the characteristic parameters of elemental superconductors, then turn to compound superconductors, which are the most important for applications, and finally present high-T_c superconductors.

26.2.1 Superconducting Elements

In Table 26.3 we listed those elements that become superconductors at normal pressure in the bulk. Besides the critical temperature, the critical magnetic

induction B_c is listed, since this is used ever more widely in the literature instead of the critical magnetic field H_c. For type II superconductors – such as niobium, tantalum, and technetium – the magnetic induction that corresponds to the *thermodynamic critical field* H_c is given. This quantity will be defined later; for now it is enough to know that it is between H_{c1} and H_{c2}.

Table 26.3. The critical temperature T_c and the critical magnetic induction B_c of superconducting elements

Element	T_c (K)	B_c (mT)	Element	T_c (K)	B_c (mT)
Al	1.18	10.5	Pa	1.4	
Am	0.6		Pb	7.20	80.3
Be	0.03	9.9	Re	1.70	20.1
Cd	0.52	2.8	Rh	3.2×10^{-4}	5×10^{-3}
Ga	1.08	5.9	Ru	0.49	6.9
Hf	0.13	1.3	Sn	3.72	30.5
α-Hg	4.15	41.1	Ta	4.47	82.9
β-Hg	3.95	33.9	Tc	7.8	141
In	3.41	28.2	Th	1.37	16.0
Ir	0.11	1.6	Ti	0.40	5.6
α-La	4.87	80	Tl	2.38	17.6
β-La	6.06	110	U	0.68	10.0
Lu	0.1	35.0	V	5.46	140
Mo	0.92	9.7	W	0.01	0.1
Nb	9.25	206	Zn	0.86	5.4
Os	0.66	7.0	Zr	0.63	4.7

Even more confusing than the inconsistent usage of B and H, the literature also lacks unanimity in the choice of units. The CGS system is still widely used, so the critical field is often given in oersteds instead of the corresponding SI unit, A/m. Other authors speak about the magnetic field but specify it in gausses or teslas. In Table 26.3 B_c is given, in milliteslas. To obtain the value of H_c in A/m, it has to be multiplied by $10^4/4\pi = 795.8$. Oersted values are obtained through $1\,\mathrm{mT} \widehat{=} 10\,\mathrm{Oe}$.

It is worth taking a look at how these superconducting materials are distributed among the groups of the periodic table. This is shown in Table 26.4.

It is no surprise that the good semiconductors in group 14 (column IVA) and the nonmetallic elements in groups 15, 16, and 17 (columns VA, VIA and VIIA) do not become superconductors at atmospheric pressure even at very low temperatures although it should be mentioned that they do so under very high pressure – ranging from about 10 GPa to over 100 GPa for oxygen, sulfur, and bromine – at a few kelvins. For example, the critical temperature reaches 18 K at 30 GPa for phosphorus. It should also be noted that at normal pres-

Table 26.4. Superconducting elements in the periodic table. Elements shown in white on black become superconductors in the bulk at atmospheric pressure, while those in italics on gray only under high pressure or in thin films

1																	18
H	2											13	14	15	16	17	He
Li	Be											*B*	*C*	N	*O*	F	Ne
Na	Mg	3	4	5	6	7	8	9	10	11	12	Al	*Si*	*P*	*S*	Cl	Ar
K	*Ca*	*Sc*	Ti	V	*Cr*	Mn	*Fe*	Co	Ni	Cu	Zn	Ga	*Ge*	*As*	*Se*	*Br*	Kr
Rb	*Sr*	*Y*	Zr	Nb	Mo	Tc	Ru	Rh	*Pd*	Ag	Cd	In	Sn	*Sb*	*Te*	*I*	Xe
Cs	*Ba*	La	Hf	Ta	W	Re	Os	Ir	Pt	Au	Hg	Tl	Pb	*Bi*	Po	At	Ra
Fr	Ra	Ac	Rf	Db	Sg	Bh	Hs	Mt									

Ce	Pr	Nd	Pm	Sm	Eu	Gd	Tb	Dy	Ho	Er	Tm	Yb	Lu
Th	Pa	U	Np	Pu	Am	Cm	Bk	Cf	Es	Fm	Md	No	Lr

sure neither alkali metals, nor alkaline-earth metals (apart from beryllium), nor noble metals are superconductors – in short, none of the simplest metals to which the free-electron model can be applied successfully. Superconductors are found among the elements of groups 12 and 13 (columns IIB and IIIA), the non-semiconductor elements of group 14 (column IVA), and transition metals. However, transition metals that are magnetically ordered, or are in a sense close to becoming magnetically ordered, do not display superconductivity. But this rule is not watertight either: at high pressure iron loses its magnetization, recrystallizes in an hcp structure, and then becomes a superconductor below 2 K. Chromium exhibits superconductivity in thin films. As we shall see in Volume 3, the presence of a uniform ferromagnetic order rules out the possibility of superconductivity. In antiferromagnetic or nonuniform ferromagnetic materials the situation is not so clear: the two kinds of order usually compete and work against each other, although there are certain cases when they coexist.

Among lanthanoides, only lanthanum and lutetium are superconductors. The critical temperature is slightly different for the two crystallographic modifications of lanthanum, α-La (hcp structure) and β-La (fcc structure). To date, four actinoids have been found to exhibit superconductivity: thorium, protactinium, uranium (α and γ modifications), and americium. With the exception of niobium, technetium, and vanadium, elemental superconductors are all type I. The lower and upper critical fields are given in Table 26.5 for these exceptions.

Table 26.5. The critical temperature T_c and the lower and upper critical fields for elemental type II superconductors

Element	T_c (K)	B_{c1} (mT)	B_{c2} (mT)
Nb	9.25	173	405
Tc	7.8	120	312
V	5.4	115	296

The critical temperature may change under high pressure. The critical temperature of zirconium changes from 0.6 K at normal pressure to 11 K at 30 GPa, while the T_c of vanadium reaches 17.2 K at 120 GPa. Several other elements – such as As, B, Ba, Bi, Ca, Ce, Cs, Fe, Ge, Li, P, Sb, Sc, Se, Si, Sr, Te, and Y – that behave as normal metals or semiconductors become superconductors under pressures of order 10^3 MPa or higher. Among all elements, the highest critical temperature was observed in lithium: $T_c = 20$ K at a pressure of 50 GPa. Even Br, I, O, and S become superconductor under very high pressure.

In other cases the superconducting parameters of amorphous samples or thin films are different from those observed in bulk crystalline samples. For example, in thin films tungsten becomes a superconductor at 5.5 K instead of 0.01 K, beryllium at 9.95 K instead of 26 mK, and gallium at 8.6 K instead of 1.08 K. Another interesting finding is that carbon becomes a superconductor in its most recently discovered allotropic modification, the nanotube, and its critical temperature depends on the tube diameter. Its highest critical temperature registered to date is 15 K.

26.2.2 Superconducting Compounds

Compared to elemental superconductors, higher critical temperatures can be found in metallic alloys or compounds. A particularly interesting family of such compounds is the group of materials of composition M_3X – where M stands for niobium or vanadium –, crystallized in A15 structure (shown in Fig. 7.5). The transition temperatures for some of them are listed in Table 26.6.

Members of this family held the record of highest transition temperature for a good while. For applications, the upper critical field may be even more important; this reaches 24.7 T in Nb_3Sn and 23 T in V_3Si. The highest critical fields occur in another family, the so-called Chevrel-phase compounds. Their generic composition is $M_xMo_6X_8$, where M is a metallic element and X is either sulfur or selenium. The transition temperature may depend strongly on the number x specifying the composition, which is not necessarily one. This is ignored in Table 26.7, in which the parameters – including typical values for T_c – are listed for a number of superconductors.

Table 26.6. Transition temperature of A15 superconductors

Compound	T_c (K)	Compound	T_c (K)
V_3Au	3.0	Nb_3Au	11.5
V_3Al	9.6	Nb_3Al	19.1
V_3Ga	16.8	Nb_3Ga	14.5
V_3In	13.9	Nb_3In	9.2
V_3Si	17.1	Nb_3Si	19.0
V_3Ge	8.2	Nb_3Ge	23.2
V_3Sn	3.8	Nb_3Sn	18.1
V_3Pt	2.9	Nb_3Pt	10.9

Table 26.7. The transition temperature and upper critical magnetic induction for Chevrel-phase superconductors

Compound	T_c (K)	B_{c2} (T)	Compound	T_c (K)	B_{c2} (T)
Mo_6S_8	1.9		Mo_6Se_8	6.5	
$LaMo_6S_8$	7.1	5.4	$LaMo_6Se_8$	11.4	44.5
$Cu_2Mo_6S_8$	10.7		$Cu_2Mo_6Se_8$	5.9	
$PbMo_6S_8$	14.7	55.0	$PbMo_6Se_8$	3.8	3.8
$TlMo_6S_8$	8.7		$TlMo_6Se_8$	12.2	
$SnMo_6S_8$	11.8	34.0	$SnMo_6Se_8$	6.8	
$YbMo_6S_8$	8.6		$YbMo_6Se_8$	5.8	

It was discovered in the early 1990s that some alkali-metal-doped fullerites (which are made up of C_{60} molecules, see page 29 of Volume 1) exhibit superconductivity. Relatively high T_c was found in alkali-metal fullerides of composition M_3C_{60}. Their transition temperatures are given in Table 26.8.

Table 26.8. Critical temperature of alkali fullerides of composition M_3C_{60}

Compound	T_c (K)	Compound	T_c (K)
K_3C_{60}	19.5	Rb_3C_{60}	29.5
K_2RbC_{60}	23.0	Rb_2CsC_{60}	31
K_2CsC_{60}	24.0	$RbCs_2C_{60}$	33
KRb_2C_{60}	27.0	Cs_3C_{60}	47

It is worth noting that the increase in the critical temperature of fullerides is directly related to the increase in the lattice constant, brought about by placing larger and larger alkali atoms in the lattice.

A rather intensely studied materials of the past years has been MgB_2, in which hcp layers of manganese atoms become intertwined with honeycomb-structured (graphite-like) layers of boron atoms. The particularly keen interest is due to the highest transition temperature ever found in "conventional"[5] superconductors: $T_c = 40\,K$.

Owing to their physical properties, heavy-fermion superconductors occupy a special place among superconducting compounds. They will be presented in Chapter 35.

26.2.3 High-Temperature Superconductors

Well into the 1980s, newer and newer superconducting materials were discovered but the highest attained critical temperature kept increasing quite slowly. Then in 1986 an observation made by J. G. Bednorz and K. A. Müller[6] triggered an unprecedented hunt for materials with higher and higher T_c. They found that by taking the semiconducting compound La_2CuO_4, which becomes antiferromagnetically ordered at $T_N = 540\,K$, and replacing a part of the trivalent La^{3+} ions by divalent Ba^{2+} or Sr^{2+} ions, the resistivity of the electron-deficient material (in which hole conduction dominates) starts to drop rapidly at a higher temperature than in previously studied materials. However, the transition was not sharp, and the electrical resistance did not vanish completely, either. The Meissner–Ochsenfeld effect could not be observed, but the measurements performed in magnetic fields indicated strong diamagnetism.

By the first months of 1987 it became clear that the materials of composition $La_{2-x}Ba_xCuO_4$become superconductors between 30 and 35 K, depending on the concentration of the Ba ions. At high pressures the critical temperature was found to be close to 40 K. Using strontium instead of barium, the critical temperature of $La_{2-x}Sr_xCuO_4$ was observed to reach 37.5 K even at normal pressures for the composition $x \approx 0.15$.

This discovery gave a new impetus to the search of superconductors with higher and higher T_c. Still in 1987 it was found that in $YBa_2Cu_3O_{7-\delta}$ (YBCO) the critical temperature, which depends on the oxygen content, can even reach 93 K. The transition was not sharp here, either, as shown in Fig. 26.2. The Meissner–Ochsenfeld effect could not be observed entirely: the samples did not become perfectly diamagnetic (that is, the susceptibility did not reach -1). Through the improvements in sample preparation during the past decades, the susceptibility of high-quality crystals is close to the ideal value of -1 now. When Y is replaced by a rare-earth metal, the transition temperature varies relatively little.

[5] As will be seen in Chapter 34, a superconductor is called *conventional* if the spin-singlet Cooper pairs responsible for superconductivity are formed by the electron–phonon interaction, and the order parameter exhibits s-wave symmetry, therefore the BCS theory can be used to describe it.

[6] See the footnote on page 6 of Volume 1.

The two families of materials are commonly called 214 and 123 compounds, referring to the ratios of the components. The critical temperature of some of them are listed in Table 26.9. Critical fields are not shown because they may depend on the direction of the applied field on account of the strong anisotropy of the sample. According to estimates, B_{c2} can be as high as 180 T in $YBa_2Cu_3O_{7-\delta}$.

Table 26.9. The transition temperatures for some members of the first discovered families of high-T_c superconductors

Compound	T_c (K)	Compound	T_c (K)
$La_{2-x}Ba_xCuO_4$	33	$YBa_2Cu_3O_{7-\delta}$	93
$La_{2-x}Sr_xCuO_4$	37.5	$LaBa_2Cu_3O_7$	89
$La_2CuO_{4+\delta}$	42	$NdBa_2Cu_3O_7$	96

These new superconductors share a number of common features. The characteristic layered structure of $La_{2-x}Sr_xCuO_4$ was shown in Fig. 7.23(b). We shall show it once again in Fig. 26.15, along with the structure of the parent compound of $YBa_2Cu_3O_{7-\delta}$.

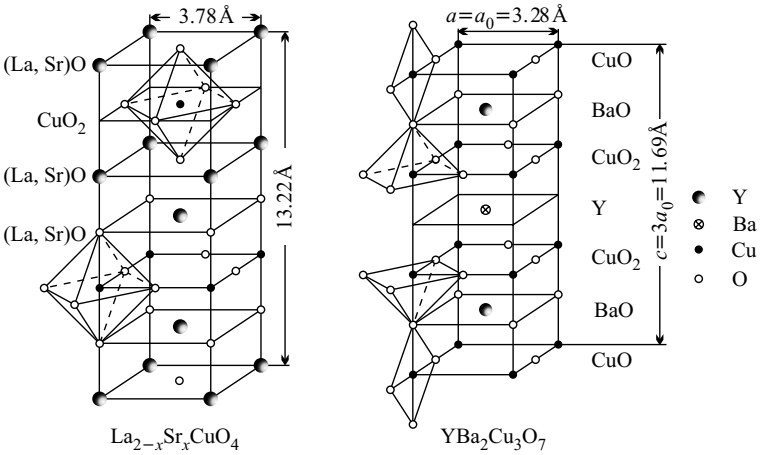

Fig. 26.15. The structure of $La_{2-x}Sr_xCuO_4$ and $YBa_2Cu_3O_7$

In both structures the copper ion and the octahedrally coordinated oxygen ions surrounding it make up Cu–O planes between the other constituents. In $La_{2-x}Sr_xCuO_4$ the La^{3+} ions sit between these planes. The Sr^{2+} (Ba^{2+}) ions only serve as a reservoir of carriers. In $YBa_2Cu_3O_{7-\delta}$ there are two Cu–O planes per primitive cell, and the oxygen deficiency provides the carriers.

More and more signs point to the conclusion that these Cu–O planes play an important role in superconductivity. That is why these families of superconductors are called cuprate superconductors.[7] In stoichiometric La_2CuO_4 the half spins of Cu^{2+} ions are coupled antiferromagnetically via superexchange through the oxygen ions, and make up an ordered antiferromagnetic structure. The situation is very similar in $YBa_2Cu_3O_{7-\delta}$ when $\delta \approx 1$. In both cases, the small variation of the concentration of one component rapidly destroys the magnetic order, and the sample becomes a superconductor. It looks as if the electrons or holes moving in the Cu–O plane, among the disordered magnetic moments, were responsible for superconductivity, and the relevant interaction between these electrons were not the same as in conventional superconductors. We shall discuss this point in detail in Chapter 34 on the microscopic theory of superconductivity.

Somewhat later appropriate technologies were developed for synthesizing material families in which the number of Cu–O planes can be controlled systematically. The materials in the series

$$\begin{aligned} HgBa_2Ca_{n-1}Cu_nO_{2n+2},\\ TlBa_2Ca_{n-1}Cu_nO_{2n+3},\\ Bi_2Sr_2Ca_{n-1}Cu_nO_{2n+4},\\ Tl_2Ba_2Ca_{n-1}Cu_nO_{2n+4} \end{aligned}$$

contain n Cu–O planes. The structures for $n = 1, 2, 3$ are shown for two of them in Figs. 26.16 and 26.17.

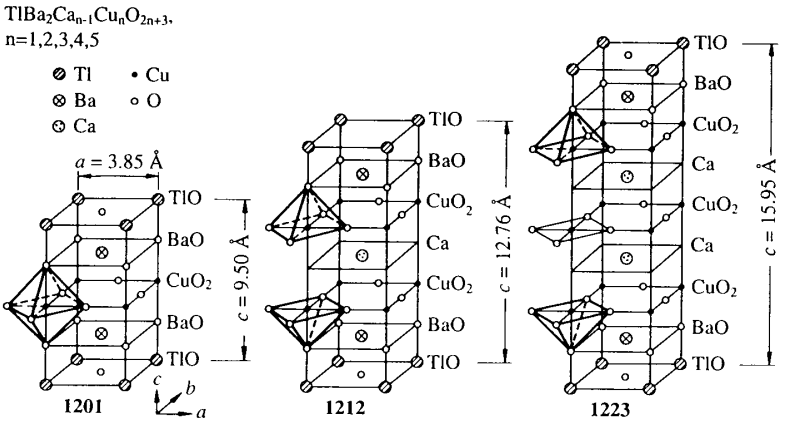

Fig. 26.16. The structure of cuprate superconductors of composition $TlBa_2Ca_{n-1}Cu_nO_{2n+3}$ for $n = 1, 2, 3$

[7] The names copper-oxide ceramic superconductors and ceramic superconductors are also used.

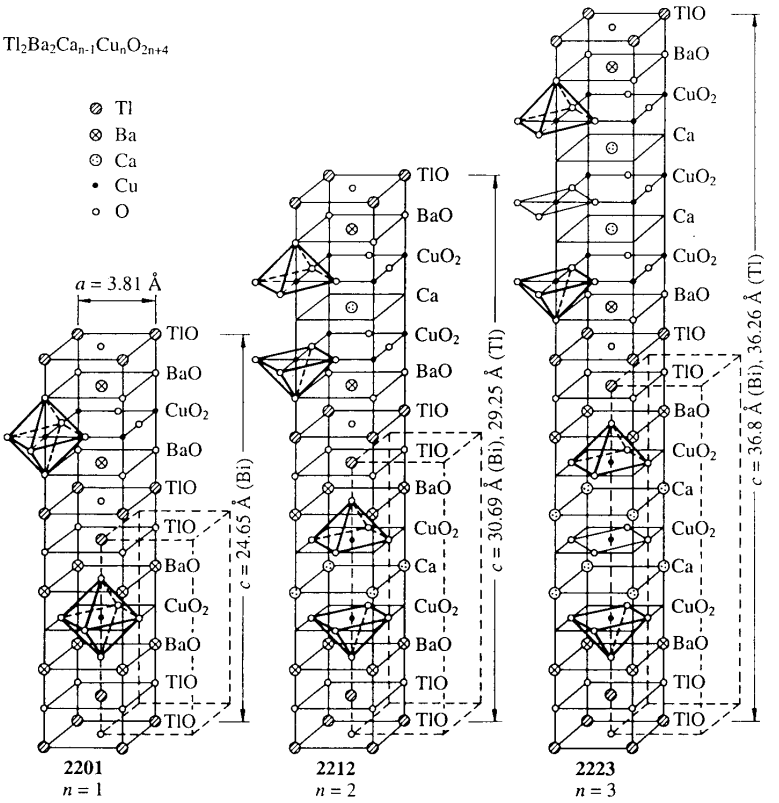

Fig. 26.17. The structure of cuprate superconductors of composition $Tl_2Ba_2Ca_{n-1}Cu_nO_{2n+4}$ for $n = 1, 2, 3$

As listed in Table 26.10, their transition temperatures increase for a while for increasing n, and then start to decrease again. The currently known highest T_c at atmospheric pressure, 138 K, was observed in the compound $Hg_{0.8}Tl_{0.2}Ba_2Ca_2Cu_3O_{8.33}$, which contains three Cu–O planes. At high pressure even higher transition temperatures can be reached: at 30 GPa $T_c = 157$ K was measured.

26.3 Phenomenological Description of Superconductivity

As was demonstrated in the previous sections, superconductors show different thermodynamic and electrodynamic behavior from normal metals. These differences can be fully understood only within the framework of the microscopic theory. Since that treatment draws heavily on the apparatus of the

Table 26.10. High-T_c superconducting compounds, their abbreviated notations, and their transition temperatures

Compound	Notation	T_c (K)
$Bi_2Sr_2CuO_6$	Bi-2201	9
$Bi_2Sr_2CaCu_2O_8$	Bi-2212	92
$Bi_2Sr_2Ca_2Cu_3O_{10}$	Bi-2223	110
$Tl_2Ba_2CuO_6$	Tl-2201	95
$Tl_2Ba_2CaCu_2O_8$	Tl-2212	118
$Tl_2Ba_2Ca_2Cu_3O_{10}$	Tl-2223	127
$Tl_2Ba_2Ca_3Cu_4O_{12}$	Tl-2234	109
$TlBa_2CaCu_2O_7$	Tl-1212	103
$TlBa_2Ca_2Cu_3O_9$	Tl-1223	133
$TlBa_2Ca_3Cu_4O_{11}$	Tl-1234	112
$TlBa_2Ca_4Cu_5O_{13}$	Tl-1245	<120
$HgBa_2CuO_4$	Hg-1201	95
$HgBa_2CaCu_2O_6$	Hg-1212	126
$HgBa_2Ca_2Cu_3O_8$	Hg-1223	135
$HgBa_2Ca_3Cu_4O_{10}$	Hg-1234	125
$HgBa_2Ca_4Cu_5O_{12}$	Hg-1245	101

many-body problem, it has to be deferred to Volume 3 (Chapter 34). Below we shall give a phenomenological description.

26.3.1 Thermodynamics of Superconductors

As follows from general thermodynamic considerations, the thermodynamic potential used to describe the properties of superconductors depends on the set of independent variables. If the magnetic properties are ignored, and the temperature T and volume V are given, the Helmholtz free energy

$$F = E - TS \tag{26.3.1}$$

has to be minimized. Likewise, when the temperature T and the pressure p are fixed, the state with the lowest value of the Gibbs free energy

$$G = E - TS + pV \tag{26.3.2}$$

is the equilibrium state.

The variation of the volume does not play an important role in superconductors – however, magnetic properties are essential. Then the work done by the magnetic field on the system needs to be taken into account in the internal-energy balance. The variation of the internal energy density is therefore given by

$$\mathrm{d}w = T\,\mathrm{d}s + \mu_0 \boldsymbol{H} \cdot \mathrm{d}\boldsymbol{M}. \tag{26.3.3}$$

Henceforth we shall systematically use lowercase symbols to denote the densities of the appropriate extensive thermodynamic quantities. The contribution $\mu_0 \boldsymbol{H} \cdot \mathrm{d}\boldsymbol{H}$ of the electromagnetic field energy has to be added to the internal energy. The variation of the internal energy density is then

$$\mathrm{d}w = T\,\mathrm{d}s + \mu_0 \boldsymbol{H} \cdot \mathrm{d}\boldsymbol{M} + \mu_0 \boldsymbol{H} \cdot \mathrm{d}\boldsymbol{H} = T\,\mathrm{d}s + \boldsymbol{H} \cdot \mathrm{d}\boldsymbol{B}. \tag{26.3.4}$$

If the magnetic induction (flux density) $\boldsymbol{B}$ is the independent, natural variable, the variation of the Helmholtz free energy density f is

$$\mathrm{d}f(T, \boldsymbol{B}) = -s\,\mathrm{d}T + \boldsymbol{H} \cdot \mathrm{d}\boldsymbol{B}. \tag{26.3.5}$$

In most experiments it is not the magnetic flux density that is controlled directly but the applied magnetic field $\boldsymbol{H}$, by means of applied currents. The relevant thermodynamic potential is then the Gibbs free energy, which is a function of T and $\boldsymbol{H}$. It is obtained from the Helmholtz free energy $F(T, \boldsymbol{B})$ by a Legendre transformation. In terms of the densities,

$$g(T, \boldsymbol{H}) = f(T, \boldsymbol{B}) - \boldsymbol{B} \cdot \boldsymbol{H}. \tag{26.3.6}$$

The behavior of the system is determined by the minimum of this quantity. The condition for thermodynamic equilibrium is

$$\left(\frac{\partial g}{\partial \boldsymbol{B}}\right)_{\boldsymbol{H}} = 0\,. \tag{26.3.7}$$

When the temperature and magnetic field are varied, the Gibbs potential changes by

$$\mathrm{d}g(T, \boldsymbol{H}) = -s\,\mathrm{d}T - \boldsymbol{B} \cdot \mathrm{d}\boldsymbol{H}. \tag{26.3.8}$$

This implies the following formulas for the entropy and magnetic induction:

$$s = -\left(\frac{\partial g}{\partial T}\right)_{\boldsymbol{H}}, \qquad \boldsymbol{B} = -\left(\frac{\partial g}{\partial \boldsymbol{H}}\right)_{T}. \tag{26.3.9}$$

Integration of (26.3.8) gives the variation of the Gibbs potential for a sample placed in a magnetic field. In isotropic systems

$$g(T, H) = g(T, 0) - \int_0^H \boldsymbol{B}(H') \cdot \mathrm{d}\boldsymbol{H}'\,. \tag{26.3.10}$$

In the normal state, if the sample itself is not magnetically ordered, $\mu_\mathrm{r} \approx 1$ and $\boldsymbol{B} = \mu_0 \boldsymbol{H}$ to a good approximation, thus

$$g_\mathrm{n}(T, H) = g_\mathrm{n}(T, 0) - \tfrac{1}{2}\mu_0 H^2. \tag{26.3.11}$$

In the superconducting state of type I superconductors $\boldsymbol{B} = 0$ in the bulk of the sample, so, if the contribution of the thin surface layer can be neglected,

$$g_{\mathrm{s}}(T,H) = g_{\mathrm{s}}(T,0)\,. \tag{26.3.12}$$

The free energy in the superconducting and normal phases are plotted against the magnetic field in Fig. 26.18.

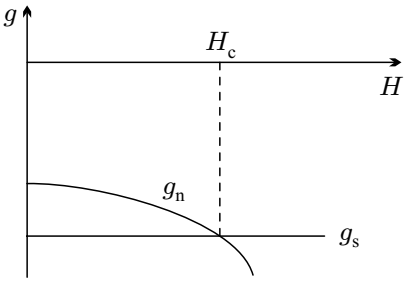

Fig. 26.18. The dependence of the Gibbs free energy on the magnetic field in the superconducting and normal phases

In the absence of an applied magnetic field the superconducting phase is stable below the critical temperature as its Gibbs free energy is lower. The difference of the free energies of the superconducting and normal phases is called the condensation energy. In the presence of a magnetic field the free energy of the normal state becomes lower, while that of the superconducting phase is left unchanged. In fields exceeding a critical strength, the Gibbs free energy is lower for the normal state than for the superconducting state. The critical magnetic field H_{c}, where the phase transition occurs, is determined by

$$g_{\mathrm{s}}(T,H_{\mathrm{c}}) = g_{\mathrm{n}}(T,H_{\mathrm{c}})\,. \tag{26.3.13}$$

Using the previous formulas,

$$g_{\mathrm{s}}(T,0) = g_{\mathrm{n}}(T,0) - \tfrac{1}{2}\mu_0 H_{\mathrm{c}}^2\,. \tag{26.3.14}$$

The condensation energy can thus be simply related to the critical field. This is particularly noteworthy because the condensation energy can be determined from the microscopic theory, and so the temperature dependence of the critical field can be derived.

The difference of the two Gibbs free energies in a magnetic field can also be written as

$$g_{\mathrm{s}}(T,H) = g_{\mathrm{n}}(T,H) + \tfrac{1}{2}\mu_0\left(H^2 - H_{\mathrm{c}}^2\right). \tag{26.3.15}$$

The entropies of the two phases at the critical field of the transition can be determined through (26.3.9), leading to

$$s_{\mathrm{s}} - s_{\mathrm{n}} = \mu_0 H_{\mathrm{c}}\,\frac{\mathrm{d}H_{\mathrm{c}}}{\mathrm{d}T}\,. \tag{26.3.16}$$

It follows from the previously derived temperature dependence of the critical field that the quantity on the right-hand side is negative, thus the entropy of

the superconducting phase is indeed lower than that of the normal phase. The latent heat of the phase transition is then

$$q = T(s_\mathrm{n} - s_\mathrm{s}) = -T\mu_0 H_\mathrm{c} \frac{\mathrm{d}H_\mathrm{c}}{\mathrm{d}T} \,. \tag{26.3.17}$$

This quantity vanishes at $T = 0$ and $T = T_\mathrm{c}$, where $H_\mathrm{c} = 0$. The transition is second order in both points and first order everywhere else.

Calculating the specific heat from $c = T\partial s/\partial T$,

$$c_\mathrm{s} - c_\mathrm{n} = T\mu_0 \left[H_\mathrm{c} \frac{\mathrm{d}^2 H_\mathrm{c}}{\mathrm{d}T^2} + \left(\frac{\mathrm{d}H_\mathrm{c}}{\mathrm{d}T} \right)^2 \right] . \tag{26.3.18}$$

It seems justified to assume that the transition to the superconducting state does not modify the phonon spectrum, so the specific-heat contribution of lattice vibrations is the same in the two phases. The jump in the specific heat is related to changes in the excitation spectrum of the electron system.

Using the empirical formula (26.1.3) for the temperature dependence of the critical field,

$$c_\mathrm{s} - c_\mathrm{n} = 6\mu_0 \frac{H_\mathrm{c}^2(0)}{T_\mathrm{c}} \left[-\frac{1}{3} \left(\frac{T}{T_\mathrm{c}} \right) + \left(\frac{T}{T_\mathrm{c}} \right)^3 \right] . \tag{26.3.19}$$

At low temperatures the second term is much smaller than the first. Since the specific heat of the superconductor is exponentially small, we may identify the term that is proportional to the temperature with the electronic contribution $c_\mathrm{n} = \gamma T$ to the specific heat of normal metals. By making use of (26.1.3) once again, we have

$$\gamma = -\mu_0 H_\mathrm{c} \frac{\mathrm{d}^2 H_\mathrm{c}}{\mathrm{d}T^2} = 2\mu_0 \left(\frac{H_\mathrm{c}(0)}{T_\mathrm{c}} \right)^2 . \tag{26.3.20}$$

According to (16.2.91), γ can be related to the electronic density of states at the Fermi energy, which can thus also be determined from the measurement of H_c and T_c.

The jump in the specific heat in the critical point is given by the *Rutgers formula*[8]

$$(c_\mathrm{s} - c_\mathrm{n})_{T_\mathrm{c}} = T_\mathrm{c}\, \mu_0 \left(\frac{\mathrm{d}H_\mathrm{c}}{\mathrm{d}T} \right)^2_{T_\mathrm{c}} = 4\mu_0 \frac{H_\mathrm{c}^2(0)}{T_\mathrm{c}} \,. \tag{26.3.21}$$

The quantities on the two sides can be measured independently. Experimental data usually obey this formula quite well.

Thermodynamic relations can also be applied to type II superconductors, even though the *thermodynamic critical field* – which is derived from the energy difference between the normal and superconducting phases – does not

[8] A. J. Rutgers, 1936.

have a direct physical meaning. In the normal phase, where the magnetic induction inside the sample is determined by $B = \mu_0 H$,

$$\frac{\partial}{\partial H}\, g_{\mathrm{n}}(T, H) = -\mu_0 H\,. \tag{26.3.22}$$

In the superconducting phase

$$\frac{\partial}{\partial H}\, g_{\mathrm{s}}(T, H) = -B \tag{26.3.23}$$

is satisfied. By combining the two equations,

$$\frac{\partial}{\partial H}\big[g_{\mathrm{n}}(T, H) - g_{\mathrm{s}}(T, H)\big] = B - \mu_0 H = \mu_0 M\,. \tag{26.3.24}$$

Thus, when the magnetization is integrated up to the upper critical field,

$$\int_0^{H_{\mathrm{c2}}} M\,\mathrm{d}H = \frac{1}{\mu_0}\big[g_{\mathrm{n}}(T, H_{\mathrm{c2}}) - g_{\mathrm{s}}(T, H_{\mathrm{c2}})\big] - \frac{1}{\mu_0}\big[g_{\mathrm{n}}(T, 0) - g_{\mathrm{s}}(T, 0)\big]. \tag{26.3.25}$$

At the upper critical field the Gibbs free energy is the same in the superconducting and normal phases, and for $H = 0$ this difference is the condensation energy. Writing this in the same form as for type I superconductors, we can introduce the thermodynamic critical field H_{c} through the definition

$$\tfrac{1}{2}\mu_0 H_{\mathrm{c}}^2 = g_{\mathrm{n}}(T, 0) - g_{\mathrm{s}}(T, 0)\,. \tag{26.3.26}$$

Then

$$\int_0^{H_{\mathrm{c2}}} M\,\mathrm{d}H = -\tfrac{1}{2} H_{\mathrm{c}}^2\,. \tag{26.3.27}$$

By measuring the equilibrium magnetization curve, a measurement instruction can be given for the determination of the thermodynamic critical field.

26.3.2 Electrodynamics of Superconductors

In 1935 the brothers Fritz and Heinz London proposed a simple system of equations for the description of the electric and magnetic properties of superconductors. They assumed that the Maxwell equations could be applied in their original form, only the constitutive relations required modification. In line with an early phenomenological theory of superconductivity, the *Gorter–Casimir two-fluid model*,[9] they considered that besides normal electrons, superconductors also contain another type of carrier, of charge $-e^*$ and mass m^*, in a number density n_{s}^*. For simplicity, we shall call them superconducting electrons in this chapter. Normal electrons participate in scattering, and

[9] C. J. Gorter and H. B. G. Casimir, 1934.

their relaxation time τ_n is finite, whereas superconducting electrons move in the sample without dissipation. Their current density can be written in the customary form

$$\boldsymbol{j}_\mathrm{s} = -e^* n_\mathrm{s}^* \boldsymbol{v}_\mathrm{s}\,, \tag{26.3.28}$$

where $\boldsymbol{v}_\mathrm{s}$ is the velocity of superconducting electrons. If this current is not dissipated, the superconducting electrons accelerate freely in an electric field; their equation of motion is

$$m^* \frac{\mathrm{d}\boldsymbol{v}_\mathrm{s}}{\mathrm{d}t} = -e^* \boldsymbol{E}\,. \tag{26.3.29}$$

The equation governing the variations of the current with time is then

$$\boxed{\frac{\mathrm{d}\boldsymbol{j}_\mathrm{s}}{\mathrm{d}t} = \frac{n_\mathrm{s}^* e^{*2}}{m^*}\boldsymbol{E}\,.} \tag{26.3.30}$$

This is the *first London equation*, which formulates the infinity of the conductivity.

Another relation is obtained by substituting this formula into the Maxwell equation

$$\operatorname{curl}\boldsymbol{E} = -\frac{\partial \boldsymbol{B}}{\partial t}\,. \tag{26.3.31}$$

This leads to

$$\frac{\mathrm{d}}{\mathrm{d}t}\left(\frac{m^*}{n_\mathrm{s}^* e^{*2}}\,\operatorname{curl}\boldsymbol{j}_\mathrm{s}\right) = -\frac{\partial \boldsymbol{B}}{\partial t}\,, \tag{26.3.32}$$

and after some rearrangement to

$$\frac{\mathrm{d}}{\mathrm{d}t}\left(\operatorname{curl}\boldsymbol{j}_\mathrm{s} + \frac{n_\mathrm{s}^* e^{*2}}{m^*}\boldsymbol{B}\right) = 0\,. \tag{26.3.33}$$

The London brothers assumed that the parenthesized expression is not only constant in time but zero, that is

$$\boxed{\operatorname{curl}\boldsymbol{j}_\mathrm{s} = -\frac{n_\mathrm{s}^* e^{*2}}{m^*}\boldsymbol{B}\,.} \tag{26.3.34}$$

This is the *second London equation*. When the magnetic induction is expressed in terms of the vector potential as $\boldsymbol{B} = \operatorname{curl}\boldsymbol{A}$,

$$\boldsymbol{j}_\mathrm{s} = -\frac{n_\mathrm{s}^* e^{*2}}{m^*}\boldsymbol{A} \tag{26.3.35}$$

is obtained, which implies a local relationship between the superconducting current and the vector potential.

By introducing the parameter

$$\lambda_{\mathrm{L}}^2 = \frac{m^*}{n_{\mathrm{s}}^* e^{*2} \mu_0}\,, \tag{26.3.36}$$

which has a dimension of length squared, the two London equations can also be written as

$$\boxed{\boldsymbol{E} = \mu_0 \lambda_{\mathrm{L}}^2 \frac{\mathrm{d}\boldsymbol{j}_{\mathrm{s}}}{\mathrm{d}t}\,, \qquad \boldsymbol{B} = -\mu_0 \lambda_{\mathrm{L}}^2 \operatorname{curl} \boldsymbol{j}_{\mathrm{s}}\,.} \tag{26.3.37}$$

In the discussion of the microscopic theory we shall see that the superconducting electrons are in fact bound electron pairs, the so-called Cooper pairs. To match this phenomenological theory with experimental results and the microscopic theory, we shall need to use $e^* = 2e$, $m^* = 2m_{\mathrm{e}}$, and $n_{\mathrm{s}}^* = n_{\mathrm{s}}/2$, where n_{s} is the actual density of superconducting electrons. Note that if the electron mass and charge, along with the actual density of electrons responsible for superconductivity were used instead of the corresponding effective parameters, a very similar formula would be obtained for λ_{L}:

$$\lambda_{\mathrm{L}}^2 = \frac{m_{\mathrm{e}}}{n_{\mathrm{s}} e^2 \mu_0}\,. \tag{26.3.38}$$

The reason behind choosing the second London equation in the form given above is that it leads naturally to the Meissner–Ochsenfeld effect. According to the Maxwell equations, in the static case

$$\frac{1}{\mu_0} \operatorname{curl} \boldsymbol{B} = \boldsymbol{j}_{\mathrm{s}}\,. \tag{26.3.39}$$

By taking the curl of both sides, and making use of the second London equation,

$$\operatorname{curl}\operatorname{curl} \boldsymbol{B} = \mu_0 \operatorname{curl} \boldsymbol{j}_{\mathrm{s}} = -\mu_0 \frac{n_{\mathrm{s}}^* e^2}{m} \boldsymbol{B} = -\frac{1}{\lambda_{\mathrm{L}}^2} \boldsymbol{B}\,. \tag{26.3.40}$$

We shall determine the solution of this equation in the special case where the $x > 0$ half-space is filled by a superconducting material and the $x < 0$ half-space by a normal metal or vacuum. By applying a uniform magnetic field in the z-direction, the magnetic induction becomes nonuniform at the superconductor side of the interface, as shown in Fig. 26.19.

As the interface is the $x = 0$ plane, all spatial variations are in the x-direction. The spatial variations of B_z are governed by

$$\frac{\mathrm{d}^2 B_z}{\mathrm{d}x^2} = \frac{1}{\lambda_{\mathrm{L}}^2} B_z\,. \tag{26.3.41}$$

We are now seeking solutions that also satisfy the auxiliary condition that the magnetic field should be B_0 in the $x < 0$ region, while deep inside the superconductor it should vanish, as required for the Meissner–Ochsenfeld effect. The result is

$$B_z(x) = \begin{cases} B_0\,, & x < 0\,, \\ B_0 \mathrm{e}^{-x/\lambda_{\mathrm{L}}}\,, & x > 0\,. \end{cases} \tag{26.3.42}$$

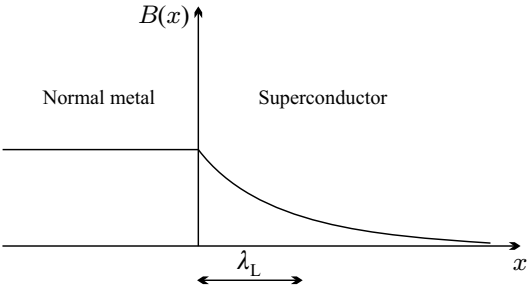

Fig. 26.19. Penetration of an applied magnetic field into the superconductor. The region is characterized by the penetration depth λ_L

Thus λ_L determines how deeply the magnetic induction can penetrate into the superconductor; only beyond that does the superconductor show the characteristic bulk behavior ($B = 0$). For this reason, λ_L is called the *London penetration depth*.

(26.3.39) implies that a surface current flows in the superconductor if the field is finite outside. The current density depends on the distance from the surface as

$$j_\mathrm{s} = j_\mathrm{s}^{(0)} \mathrm{e}^{-x/\lambda_\mathrm{L}} = \frac{1}{\mu_0 \lambda_\mathrm{L}} B_0 \mathrm{e}^{-x/\lambda_\mathrm{L}} . \tag{26.3.43}$$

This surface current screens the external magnetic field inside the superconductor. The critical current – which is the highest current that can be passed through a superconducting wire of radius R without the sample becoming a normal conductor – is then straightforward to determine. Since the current can flow only close to the surface, practically within a layer of thickness λ_L, the current is approximately

$$I = 2\pi R \lambda_\mathrm{L} j_\mathrm{s}^{(0)} . \tag{26.3.44}$$

On the other hand, the current density on the surface cannot be larger than the value associated with the critical field outside the sample, so $j_\mathrm{s}^{(0)}$ cannot exceed

$$j_\mathrm{c} = \frac{1}{\mu_0 \lambda_\mathrm{L}} B_\mathrm{c} . \tag{26.3.45}$$

The critical current is then

$$I_\mathrm{c} = 2\pi R B_\mathrm{c} / \mu_0 . \tag{26.3.46}$$

As the density of superconducting electrons is temperature dependent, so is the London penetration depth. Assuming that at $T = 0$ all electrons become superconducting – that is, n_s^* can be identified with the density of conduction electrons –, λ_L is expected to be on the order of 100 nm (1000 Å) for typical metallic electron densities. The extrapolated zero-temperature value of the measured penetration depth is given in Table 26.11 for a number of

superconductors. The measured values are in order-of-magnitude agreement with the estimated values given above.

Table 26.11. The experimental values for the penetration depth and coherence length in certain superconductors

Element	λ_{L} (nm)	ξ_0 (nm)	Compound	λ_{L} (nm)	ξ_0 (nm)
Al	45	1550	Nb_3Sn	65	3
Cd	110	760	Nb_3Ge	90	3
In	40	360	V_3Si	60	3
Nb	52	39	$PbMo_6S_8$	200	2
Pb	39	87	K_3C_{60}	240	2.6
Sn	42	180	UBe_{13}	400	7

According to the Gorter–Casimir two-fluid model, the density of normal electrons is proportional to the fourth power of T at finite temperatures, so the density of superconducting electrons is given by

$$n_{\mathrm{s}} = n_0\big[1 - (T/T_{\mathrm{c}})^4\big]\,. \tag{26.3.47}$$

The approximate formula for the temperature dependence of the penetration depth is therefore

$$\lambda_{\mathrm{L}}(T) = \lambda_{\mathrm{L}}(0)\big[1 - (T/T_{\mathrm{c}})^4\big]^{-1/2}, \tag{26.3.48}$$

in fair agreement with measurements. As the critical point is approached, the penetration depth diverges as the inverse square root of $T_{\mathrm{c}} - T$.

In high-T_{c} superconductors the penetration depth and coherence length exhibit strong anisotropy because of the layered structure. Some relevant data are listed in Table 26.12.

Table 26.12. The experimental values for the penetration depth and coherence length in two high-T_{c} cuprate superconductors, parallel and perpendicular to the Cu–O planes

Compound	$\lambda_{\parallel}$ (nm)	$\lambda_{\perp}$ (nm)	$\xi_{\parallel}$ (nm)	$\xi_{\perp}$ (nm)
$YBa_2Cu_3O_7$	100	500	1.2	0.3
$HgBa_2Ca_2Cu_3O_{10}$	130	3500	1.5	0.2

26.3.3 Pippard Coherence Length

The measured value of the penetration depth is often larger than the prediction of the London equation (26.3.36). The reason for this is that the second London equation assumes a local relationship between the current density of superconducting electrons and the vector potential. However, this assumption is too strong, and is not satisfied in all superconductors. In analogy to the Reuter–Sondheimer theory[10] of the anomalous skin effect, which led to a nonlocal generalization of Ohm's law, A. B. Pippard (1953) proposed to replace the local London equation with a nonlocal relationship, in which the current at point $\boldsymbol{r}$ does not depend on the vector potential in $\boldsymbol{r}$ alone but on its values $\boldsymbol{A}(\boldsymbol{r}')$ over a region of radius ξ_0 around $\boldsymbol{r}$. Based on Chambers' formula,[11]

$$\boldsymbol{j}(\boldsymbol{r}) = \frac{3\sigma}{4\pi l} \int \frac{\boldsymbol{R}[\boldsymbol{R}\cdot\boldsymbol{E}(\boldsymbol{r}')]}{R^4} \exp(-R/l)\,\mathrm{d}\boldsymbol{r}' \tag{26.3.49}$$

for the anomalous skin effect, where $\boldsymbol{R} = \boldsymbol{r} - \boldsymbol{r}'$, $R = |\boldsymbol{R}|$, σ is the macroscopic conductivity, and l is the mean free path, Pippard assumed

$$\begin{aligned} \boldsymbol{j}_\mathrm{s}(\boldsymbol{r}) &= -\frac{3n_\mathrm{s}e^2}{4\pi\xi_0 m_\mathrm{e}} \int \frac{\boldsymbol{R}[\boldsymbol{R}\cdot\boldsymbol{A}(\boldsymbol{r}')]}{R^4} \exp(-R/\xi_0)\,\mathrm{d}\boldsymbol{r}' \\ &= -\frac{3}{4\pi\mu_0}\frac{1}{\xi_0\lambda_\mathrm{L}^2} \int \frac{\boldsymbol{R}[\boldsymbol{R}\cdot\boldsymbol{A}(\boldsymbol{r}')]}{R^4} \exp(-R/\xi_0)\,\mathrm{d}\boldsymbol{r}' \end{aligned} \tag{26.3.50}$$

for superconductors. The temperature-independent characteristic length ξ_0 is the *Pippard coherence length*.

To estimate its value, we shall assume that the superconducting state is due dominantly to the electrons in the region of width $k_\mathrm{B}T_\mathrm{c}$ around the Fermi energy. The uncertainty of the momentum is then $\Delta p \approx k_\mathrm{B}T_\mathrm{c}/v_\mathrm{F}$. The position uncertainty

$$\Delta x \geq \hbar/\Delta p = \frac{\hbar v_\mathrm{F}}{k_\mathrm{B}T_\mathrm{c}} \tag{26.3.51}$$

implied by the Heisenberg uncertainty principle can then be identified with the coherence length ξ_0. According to the microscopic theory, its more accurate value can be expressed in terms of the energy gap Δ_0 – which is of the same order of magnitude as $k_\mathrm{B}T_\mathrm{c}$:

$$\xi_0 = \frac{\hbar v_\mathrm{F}}{\pi\Delta_0} = a\frac{\hbar v_\mathrm{F}}{k_\mathrm{B}T_\mathrm{c}}\,, \tag{26.3.52}$$

where $a \approx 0.180$. Its experimental values for a number of materials are listed in Tables 26.11 and 26.12. Visibly, ξ_0 can be two orders of magnitude larger or smaller than the London penetration depth. This plays an important role in the classification of superconductors.

[10] G. E. H. Reuter and E. H. Sondheimer, 1948.
[11] R. G. Chambers, 1952.

If $\lambda_{\mathrm{L}} \gg \xi_0$, then $\boldsymbol{A}(\boldsymbol{r})$ varies little over the interesting part of the domain of integration in (26.3.50), and a local relationship between the current density and the vector potential expressed by the second London equation is recovered. In this case the penetration of the magnetic field is determined by λ_{L} alone. As we shall see later, such a situation is encountered in type II superconductors, which are therefore also called London superconductors.

In the opposite limit, which is typical of type I superconductors, Pippard's nonlocal relationship between the current and the vector potential has to be used. That is why type I superconductors are sometimes referred to as Pippard superconductors. The actual penetration depth – the distance over which the vector potential falls off – has to be determined self-consistently. Owing to the sharp decrease of the vector potential, the integral in (26.3.50) is reduced roughly by a factor of order λ/ξ_0:

$$\boldsymbol{j}_{\mathrm{s}}(\boldsymbol{r}) = -\frac{\lambda}{\xi_0}\frac{1}{\mu_0\lambda_{\mathrm{L}}^2}\boldsymbol{A}(\boldsymbol{r})\,. \tag{26.3.53}$$

When the penetration depth is determined from this relation using the Maxwell equations, $\lambda/(\xi_0\lambda_{\mathrm{L}}^2)$ must be identified with $1/\lambda^2$. This gives

$$\lambda = \lambda_{\mathrm{L}}^{2/3}\xi_0^{1/3}\,, \tag{26.3.54}$$

which is larger than the London value, in agreement with the measurements.

When impurities are present, and the mean free path of electrons is l because of impurity scattering, the actual coherence length is given by

$$\frac{1}{\xi} = \frac{1}{\xi_0} + \frac{1}{l}\,. \tag{26.3.55}$$

In the very imperfect (dirty) limit $l \ll \xi_0$, and thus the exponential factor in the Pippard formula is $\mathrm{e}^{-|\boldsymbol{r}|/l}$. By evaluating the integral, the current and the vector potential are now related through

$$\boldsymbol{j}_{\mathrm{s}}(\boldsymbol{r}) = -\frac{l}{\xi_0}\frac{1}{\mu_0\lambda_{\mathrm{L}}^2}\boldsymbol{A}(\boldsymbol{r})\,. \tag{26.3.56}$$

The actual penetration depth of the magnetic field is then obtained from

$$\frac{l}{\xi_0}\frac{1}{\lambda_{\mathrm{L}}^2} = \frac{1}{\lambda^2}\,, \tag{26.3.57}$$

which gives

$$\lambda = \lambda_{\mathrm{L}}\left(\frac{\xi_0}{l}\right)^{1/2}. \tag{26.3.58}$$

26.3.4 Flux Quantization

The condition that the current should vanish inside the superconductor immediately implies the property mentioned among the experimental findings: the magnetic flux through a ring cannot take any arbitrary value, only the integral multiples of a flux quantum Φ_0. To demonstrate this, we have to start with the Bohr quantization condition

$$\oint_C \boldsymbol{p} \cdot \mathrm{d}\boldsymbol{l} = nh\,, \tag{26.3.59}$$

where the line integral is along some closed path. As discussed in Chapter 3, the canonical momentum $\boldsymbol{p}$ and the kinetic momentum $m^*\boldsymbol{v}_\mathrm{s}$ that determines the kinetic energy are related by

$$\boldsymbol{p} = m^*\boldsymbol{v}_\mathrm{s} - e^*\boldsymbol{A}\,. \tag{26.3.60}$$

Substituting this into the quantization condition,

$$m^* \oint_C \boldsymbol{v}_\mathrm{s} \cdot \mathrm{d}\boldsymbol{l} - e^* \oint_C \boldsymbol{A} \cdot \mathrm{d}\boldsymbol{l} = nh\,. \tag{26.3.61}$$

Expressing the velocity in terms of the current of superconducting electrons and rearranging the terms gives

$$\frac{m^*}{n_\mathrm{s}^* e^{*2}} \oint_C \boldsymbol{j}_\mathrm{s} \cdot \mathrm{d}\boldsymbol{l} + \oint_C \boldsymbol{A} \cdot \mathrm{d}\boldsymbol{l} = \frac{|n|h}{e^*}\,. \tag{26.3.62}$$

If the ring is sufficiently thick for that no current can flow in its interior, the integration path can be chosen in such a way that the contribution of the first term on the left-hand side be zero. According to Stokes' theorem, the second term is the magnetic flux Φ through a surface F bounded by the closed curve C:

$$\oint_C \boldsymbol{A} \cdot \mathrm{d}\boldsymbol{l} = \int_F \mathrm{curl}\,\boldsymbol{A}\,\mathrm{d}F = \Phi\,. \tag{26.3.63}$$

So the magnetic flux through the superconducting ring can take only discrete values, namely, the integral multiples of the flux quantum

$$\boxed{\Phi_0 = \frac{h}{e^*}\,.} \tag{26.3.64}$$

To establish agreement with the measurement shown in Fig. 26.6, e^* must be chosen as twice the elementary charge.

When the region is chosen in such a way that current flows on its boundary, then the quantization condition (in units of h/e^*) does not apply to the magnetic flux but to the fluxoid

$$\Phi + \frac{m^*}{n_\mathrm{s}^* e^{*2}} \oint\limits_C \boldsymbol{j}_\mathrm{s} \cdot \mathrm{d}\boldsymbol{l}\,, \tag{26.3.65}$$

which also contains the contribution of the superconducting current.

26.4 Ginzburg–Landau Theory

By complementing the general thermodynamic relations by a simple assumption about the temperature dependence of the critical field, and extending the Maxwell equations to the superconducting phase by means of the London equations, we gave a quite simple description of the thermodynamics and electrodynamics of the superconducting state in the previous section. The phase transition was studied through the comparison of the free energy of the normal and superconducting states, both of which were assumed to be homogeneous. If the sample is allowed to be inhomogeneous, i.e., normal and superconducting regions can alternate in it – a possibility that was mentioned as an empirical fact in connection with the Shubnikov phase of type II superconductors – then simple (and, as we shall see, naive) considerations straightforwardly lead to the conclusion that the homogeneous superconducting state can never be stable energetically. To demonstrate this, assume that normal and superconducting layers alternate inside the sample in such a way that the normal layers are much thinner than the superconducting ones, but even the thickness of the latter is smaller than the penetration length. In this geometry the normal regions contribute negligibly to the total free energy, however, they allow the magnetic field to penetrate into the superconducting regions, too. This way, the Gibbs free energy of homogeneous superconductors could be reduced. Moreover, superconductivity would not disappear at the critical field H_c (which is related to the condensation energy of bulk superconductors): it could persist in a configuration where thin superconducting and normal layers are stacked because the destruction of superconductivity requires a higher critical field in thin films than in bulk samples.

The existence of type I superconductors is in contradiction with this naive expectation. In type II superconductors the alternation of normal and superconducting regions is indeed observed between the upper and lower critical fields, however, homogeneous superconductivity is found below $H_{\mathrm{c}1}$ here, too. This indicates the necessity of a more precise study of normal metal–superconductor interfaces, most notably their energy. This requires a better treatment of superconductivity than the one based on the London equations.

This theory, called the *Ginzburg–Landau theory*, is the generalization of Landau's theory of second-order phase transitions to inhomogeneous superconductors in a magnetic field. The fundamental assumptions of Landau's theory were presented in Chapter 14. Using that as a starting point, we shall now derive the Ginzburg–Landau equations, and then use them to describe

the macroscopic properties and the vortices that appear in the intermediate state of type II superconductors.

26.4.1 Ginzburg–Landau Equations

In 1950, before the advent of the microscopic theory of superconductivity, V. L. Ginzburg[12] and L. D. Landau generalized the Landau theory of second-order phase transitions to the normal–superconducting transition. They assumed that the superconducting phase can be characterized by an order parameter that is finite only in the ordered, superconducting phase, and varies continuously below the critical point, staring from zero at T_c. They also assumed that a free-energy functional can be defined in the vicinity of the phase-transition point, and it can be expanded in powers of the order parameter. The equilibrium value of the order parameter can be determined from the minimum of the functional, whereas the actual value of the free energy is given by the value of the functional at the equilibrium order parameter.

As the magnetic field is known to penetrate into type II superconductors inhomogeneously, we shall use the free-energy-density formula (14.5.17), which takes the spatial variations of the order parameter into account, too. Besides, Ginzburg and Landau assumed that the order parameter is somehow related to the wavefunction of superconducting electrons, and is therefore a complex quantity. Their second, even more important assumption was that the term containing the gradient of the order parameter in the series expansion of the free-energy density can be considered to be related to the kinetic energy of superconducting electrons. This physical insight then implied that, just like for an electron in a magnetic field, the effects of the magnetic field have to be taken into account by replacing the canonical momentum operator $-\mathrm{i}\hbar\boldsymbol{\nabla}$ by the kinetic momentum operator, which also contains the vector potential and the charge $-e^*$ of superconducting electrons.[13] The free-energy density of the superconducting state is then

$$f_\mathrm{s} = f_\mathrm{n} + \alpha(T)|\psi|^2 + \frac{1}{2}\beta(T)|\psi|^4 + \frac{1}{2m^*}\left|\left(\frac{\hbar}{\mathrm{i}}\boldsymbol{\nabla} + e^*\boldsymbol{A}\right)\psi\right|^2 + \frac{1}{2\mu_0}\boldsymbol{B}^2\,, \quad (26.4.1)$$

where the last term is the energy of the magnetic field $\boldsymbol{B} = \operatorname{curl}\boldsymbol{A}$. In their approach the magnetic induction (or the vector potential) is fixed, which is why the Helmholtz free energy is studied.

[12] Well after the death of Landau (1908–1968), who was awarded the Nobel Prize in 1962 (see footnote on page 28 of Volume 1), Vitaly Lazarevich Ginzburg (1916–) shared the Nobel Prize with Alexei Alexeevich Abrikosov (1928–) and Anthony James Leggett (1938–) in 2003 "for pioneering contributions to the theory of superconductors and superfluids".

[13] The free energy is gauge invariant only if a universal value is taken for the charge. Ginzburg and Landau argued that there was no reason to choose it to be different from the electron charge. It is now known that e^* should be chosen as $2e$, a universal value for all superconductors.

Since the order parameter of the superconducting state has to vanish in the normal state – in other words, the free-energy minimum must be at $\psi = 0$ in the normal phase and at some nonzero value in the superconducting state –, the phase transition occurs at that temperature T_c for which $\alpha(T_\mathrm{c}) = 0$. The parameter α is positive above T_c and negative below it. Assuming a linear temperature dependence in the vicinity of the transition point,

$$\alpha(T) = a(T - T_\mathrm{c})\,, \qquad a > 0\,, \tag{26.4.2}$$

while β is chosen to be positive and temperature independent.

The spatial distribution of the order parameter and magnetic induction can be determined from the minimum of the free energy. Since the order parameter is complex, the real and imaginary parts need to be varied separately – or else, the minimum can also be sought with respect to ψ and its conjugate. The variation of the free energy is

$$\begin{aligned}\delta F_\mathrm{s} = \int \mathrm{d}\boldsymbol{r} \Bigg[& \alpha\psi\,\delta\psi^* + \beta|\psi|^2\psi\,\delta\psi^* \\ & + \frac{1}{2m^*}\left(-\frac{\hbar}{\mathrm{i}}\boldsymbol{\nabla} + e^*\boldsymbol{A}\right)\delta\psi^*\left(\frac{\hbar}{\mathrm{i}}\boldsymbol{\nabla} + e^*\boldsymbol{A}\right)\psi + \text{c.c.}\Bigg] \\ & + \int \mathrm{d}\boldsymbol{r}\left[\frac{\boldsymbol{B}}{2\mu_0}\operatorname{curl}\delta\boldsymbol{A} + \frac{e^*}{2m^*}\psi^*\delta\boldsymbol{A}\left(\frac{\hbar}{\mathrm{i}}\boldsymbol{\nabla} + e^*\boldsymbol{A}\right)\psi + \text{c.c.}\right].\end{aligned} \tag{26.4.3}$$

Integrating the terms containing the derivative of $\delta\psi^*$ and $\delta\boldsymbol{A}$ by parts,

$$\begin{aligned}\delta F_\mathrm{s} = & \int \mathrm{d}\boldsymbol{r}\left\{\delta\psi^*\left[\alpha\psi + \beta|\psi|^2\psi + \frac{1}{2m^*}\left(\frac{\hbar}{\mathrm{i}}\boldsymbol{\nabla} + e^*\boldsymbol{A}\right)^2\psi\right] + \text{c.c.}\right\} \\ & + \int \mathrm{d}\boldsymbol{r}\left\{\delta\boldsymbol{A}\left[\frac{\operatorname{curl}\boldsymbol{B}}{2\mu_0} + \frac{e^*}{2m^*}\psi^*\left(\frac{\hbar}{\mathrm{i}}\boldsymbol{\nabla} + e^*\boldsymbol{A}\right)\psi\right] + \text{c.c.}\right\}.\end{aligned} \tag{26.4.4}$$

In addition to that, the integrated part gives a surface term

$$\int \mathrm{d}\boldsymbol{S}\left[\delta\psi^*\left(\frac{\hbar}{\mathrm{i}}\boldsymbol{\nabla} + e^*\boldsymbol{A}\right)\psi + \text{c.c.}\right]. \tag{26.4.5}$$

In the calculus of variations boundary conditions have to be specified, too. Customarily, ψ and its variation are both assumed to vanish at the boundaries. Instead, Ginzburg and Landau proposed the condition of vanishing current through the surface. This condition is fulfilled when the component of the integrand along the surface normal $\boldsymbol{n}$ satisfies

$$\boldsymbol{n}\cdot\left(\frac{\hbar}{\mathrm{i}}\boldsymbol{\nabla} + e^*\boldsymbol{A}\right)\psi = 0 \tag{26.4.6}$$

on the boundary. This indeed leads to the correct result for superconductor–insulator interfaces. The situation is not so simple for superconductor–normal

metal interfaces. Since the wavefunction ψ can penetrate into the normal metal,[14] the condition that no current should flow through the surface could also be satisfied by the boundary condition

$$\boldsymbol{n} \cdot \left(\frac{\hbar}{\mathrm{i}} \boldsymbol{\nabla} + e^* \boldsymbol{A} \right) \psi = \mathrm{i} b \psi \,, \tag{26.4.7}$$

where b is real. An even more general choice is required for SIS junctions, in which the current can flow from one superconductor into the other through a thin insulating layer.

At the minimum of the free energy the bracketed terms in (26.4.4) must vanish. The *first Ginzburg–Landau equation* is obtained by equating the coefficient of $\delta\psi^*$ to zero:

$$\boxed{\frac{1}{2m^*} \left(\frac{\hbar}{\mathrm{i}} \boldsymbol{\nabla} + e^* \boldsymbol{A} \right)^2 \psi + \alpha\psi + \beta|\psi|^2\psi = 0 \,.} \tag{26.4.8}$$

Formally, this equation is a Schrödinger equation for the wavefunction ψ of superconducting electrons, in which the term proportional to $|\psi|^2$ is the potential due to the other electrons. In this sense the first Ginzburg–Landau equation is a nonlinear Schrödinger equation.

The *second Ginzburg–Landau equation* is derived from the requirement that the coefficient of $\delta\boldsymbol{A}$ also vanish, using the Maxwell equation for the current. It reads

$$\boxed{\frac{1}{\mu_0} \mathrm{curl}\, \boldsymbol{B} = \boldsymbol{j} = -\frac{e^*}{2m^*} \psi^* \left(\frac{\hbar}{\mathrm{i}} \boldsymbol{\nabla} + e^* \boldsymbol{A} \right) \psi + \mathrm{c.c.}} \tag{26.4.9}$$

This is just the quantum mechanical current formula, with $\boldsymbol{p}$ replaced by $\boldsymbol{p} + e^*\boldsymbol{A}$. The charge current is obtained by multiplying the quantum mechanical (particle) current by $-e^*$. In conjunction with the relation $\boldsymbol{B} = \mathrm{curl}\, \boldsymbol{A}$ between the vector potential and the magnetic induction, these Ginzburg–Landau equations determine the values of the order parameter ψ and magnetic induction $\boldsymbol{B}$ in the superconducting phase – and by way of it, the current as well.

The Ginzburg–Landau equations were derived phenomenologically. It was pointed out by L. P. Gorkov in 1959 that they can also be derived from the microscopic theory, and it was then established that the starred parameters have to be chosen as $e^* = 2e$ and $m^* = 2m_\mathrm{e}$ (as mentioned on page 476), since they are related to the Cooper pairs.

26.4.2 Gauge Symmetry Breaking

Suppose that a solution of the Ginzburg–Landau equations, the wavefunction $\psi(\boldsymbol{r})$ plus the vector potential $\boldsymbol{A}(\boldsymbol{r})$, is known. Since in both equations the operator

[14] This gives rise to the so-called *proximity effect*.

$$\frac{\hbar}{\mathrm{i}}\boldsymbol{\nabla} + e^*\boldsymbol{A} \tag{26.4.10}$$

acts on the wavefunction $\psi(\boldsymbol{r})$,

$$\begin{aligned} \psi'(\boldsymbol{r}) &= \psi(\boldsymbol{r})\mathrm{e}^{\mathrm{i}\phi(\boldsymbol{r})}\,, \\ \boldsymbol{A}'(\boldsymbol{r}) &= \boldsymbol{A}(\boldsymbol{r}) - \frac{\hbar}{e^*}\boldsymbol{\nabla}\phi(\boldsymbol{r}) = \boldsymbol{A}(\boldsymbol{r}) - \frac{\Phi_0}{2\pi}\boldsymbol{\nabla}\phi(\boldsymbol{r}) \end{aligned} \tag{26.4.11}$$

is also a solution – with the same energy, magnetic induction, and current.

The transformation that connects the solutions is the well-known gauge transformation of electrodynamics, and the existence of equivalent solutions is the consequence of deriving the Ginzburg–Landau equations from a gauge-invariant free energy. Among the infinitely many solutions one is chosen by nature – just like for the rotationally symmetric Heisenberg model in which a broken-symmetry state is realized with the magnetization pointing in a well-defined direction. Similarly, gauge symmetry is broken in the superconducting state.

According to Goldstone's theorem (Section 6.3.2), the breaking of a continuous symmetry implies the existence of bosonic elementary excitations with a gapless energy spectrum. However, the theorem is valid only for short-ranged forces. Owing to the lack of screening, the Coulomb interaction remains long-ranged in superconductors, so Goldstone's theorem does not apply to superconductors.

One would think that the phase of the wavefunction, which is a typical microscopic quantum mechanical quantity, cannot be measured, and is therefore of limited importance. This is indeed so for an isolated superconductor. However, when there is a weak contact between two superconductors, which prevents the establishment of thermodynamic equilibrium but allows the transfer of electrons from one superconductor to the other, their phase difference can lead to interesting phenomena. We shall return to this point at the end of the chapter.

26.4.3 Coherence Length and Penetration Depth

Based on the London equations, we have already introduced a characteristic length of the superconducting state: the penetration depth of the magnetic field. We have also mentioned that there is another characteristic length, the coherence length. In order to interpret both of them in the framework of the Ginzburg–Landau theory, we have to examine what happens close to the surface of superconductors.

Outside the superconductor the order parameter vanishes, while deep in its interior it takes the equilibrium value. Close to the surface, its variation occurs over a region of finite width ξ. To determine this parameter, consider the first Ginzburg–Landau equation in zero magnetic field:

$$-\frac{\hbar^2}{2m^*}\boldsymbol{\nabla}^2\psi + \alpha\psi + \beta|\psi|^2\psi = 0\,. \tag{26.4.12}$$

Far from the surface, where the superconductor can be considered homogeneous, the equilibrium value of the order parameter can be obtained from

$$|\psi_0|^2 = -\frac{\alpha}{\beta} \tag{26.4.13}$$

according to (14.5.4). In terms of the dimensionless quantity $f = \psi/|\psi_0|$, (26.4.12) reads

$$-\frac{\hbar^2}{2m^*}\boldsymbol{\nabla}^2 f + \alpha f - \alpha|f|^2 f = 0\,. \tag{26.4.14}$$

It follows from the division of this equation by α that the parameter ξ of dimension length defined through

$$\xi^2 = -\frac{\hbar^2}{2m^*\alpha} \tag{26.4.15}$$

characterizes the spatial variations of f. This implies that when the order parameter varies in space, e.g., it grows from zero to its equilibrium value, all spatial variations occur on the length scale determined by ξ. In order to distinguish it from the temperature-independent Pippard coherence length ξ_0, ξ is called the Ginzburg–Landau correlation length. It can be shown in the microscopic theory that the two are not independent of one another. Although the Ginzburg–Landau theory is valid only in the vicinity of the transition point, $\xi(T)$, the characteristic length of the variations of the superconducting order parameter, and ξ_0, the parameter that appears in the electrodynamics of superconductors, can both be defined in the microscopic theory. It turns out that for pure superconductors

$$\xi(T \to 0) = \xi_0\,. \tag{26.4.16}$$

It follows from our assumption about the temperature dependence of the coefficient α in the Landau expansion that the Ginzburg–Landau coherence length diverges in the critical point:

$$\xi(T) = \sqrt{\frac{\hbar^2}{2m^*a}}\,(T_\mathrm{c} - T)^{-1/2}\,. \tag{26.4.17}$$

According to the microscopic theory,

$$\xi(T) = 0.74\,\xi_0(1 - T/T_\mathrm{c})^{-1/2} \tag{26.4.18}$$

for clean superconductors, while for very imperfect ones, in the "dirty" limit

$$\xi(T) = 0.855\,(\xi_0 l)^{1/2}(1 - T/T_\mathrm{c})^{-1/2}\,. \tag{26.4.19}$$

The spatial variations of the order parameter can be determined explicitly when the surface is an infinite plane. Choosing it as the $x = 0$ plane, all variations are along the x-direction, and the governing equation is

$$\xi^2 \frac{\mathrm{d}^2 f}{\mathrm{d}x^2} = -f + f^3 = -f\left(1 - f^2\right). \tag{26.4.20}$$

This equation can be integrated exactly when both sides are multiplied by $2\,\mathrm{d}f/\mathrm{d}x$. The result is

$$\xi^2 \left(\frac{\mathrm{d}f}{\mathrm{d}x}\right)^2 = \tfrac{1}{2}\left(1 - f^2\right)^2. \tag{26.4.21}$$

Rearrangement then leads to

$$\frac{\mathrm{d}f}{\mathrm{d}x} = \frac{1}{\sqrt{2}\xi}\left(1 - f^2\right), \tag{26.4.22}$$

which can be integrated once again. The final solution is

$$f(x) = \tanh \frac{x - x_0}{\sqrt{2}\xi}, \tag{26.4.23}$$

where x_0 is a constant not specified by the equations: the position coordinate of that point inside the normal metal where the order parameter would vanish if the formula valid for the superconductor were extrapolated. Toward the sample interior, the order parameter of the superconducting state indeed increases to the equilibrium value over a characteristic length ξ, as shown in Fig. 26.20.

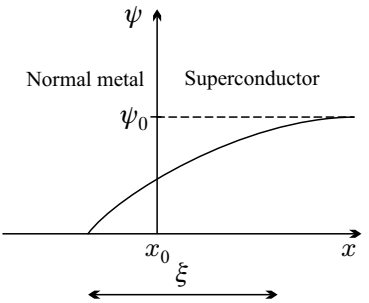

Fig. 26.20. Spatial variation of the superconducting order parameter at a normal metal–superconductor interface

The other characteristic length is the penetration depth, which was introduced and interpreted through the phenomenological London equations. We shall now show that the second London equation, which formulates the

local relationship between the current and the vector potential, can be obtained from the second Ginzburg–Landau equation if the length scale ξ of the spatial variations of the wavefunction is small compared to the characteristic scale of the variations of the magnetic field. Writing $\psi(\boldsymbol{r})$ as $|\psi(\boldsymbol{r})|\mathrm{e}^{\mathrm{i}\phi(\boldsymbol{r})}$, the superconducting current is

$$\boldsymbol{j}(\boldsymbol{r}) = -\frac{e^{*2}}{m^*}|\psi(\boldsymbol{r})|^2 \left[\boldsymbol{A}(\boldsymbol{r}) + \frac{\hbar}{e^*}\boldsymbol{\nabla}\phi(\boldsymbol{r})\right]. \tag{26.4.24}$$

This formula is very similar to (26.3.35), the formula for the local relationship between the current and the vector potential obtained from the London equation, as the second term in

$$\boldsymbol{A}(\boldsymbol{r}) + \frac{\hbar}{e^*}\boldsymbol{\nabla}\phi(\boldsymbol{r}), \tag{26.4.25}$$

which contains the gradient of the phase, can be transformed away by a gauge transformation. Instead of the density of the superconducting electrons, the previous formula contains $|\psi(\boldsymbol{r})|^2$, in complete agreement with the quantum mechanical interpretation of the wavefunction. Since ξ is assumed to be small compared to the characteristic scale of the variations of the vector potential, $|\psi(\boldsymbol{r})|$ can be approximated by the equilibrium value $|\psi_0|$. Inserting the current density into the Maxwell equations, we obtain a temperature-dependent London penetration depth defined by

$$\lambda_{\mathrm{L}}^2(T) = \frac{m^*}{\mu_0 e^{*2}|\psi_0|^2} = -\frac{m^*\beta}{\mu_0 e^{*2}\alpha} = \frac{m^*\beta}{\mu_0 e^{*2}a(T_{\mathrm{c}} - T)}. \tag{26.4.26}$$

The penetration depth diverges with the same exponent at the critical temperature as the coherence length.

26.4.4 Flux Quantization

As demonstrated in Sections 26.1.3 and 26.3.4, the magnetic flux through a superconducting ring cannot take any arbitrary value only the integral multiples of an elementary flux quantum. We shall derive this condition from the Ginzburg–Landau equations now.

Consider a non-simply connected superconductor in which the superconducting region surrounds normals regions (holes). When the sample is placed in a magnetic field, the flux lines pass through the normal region. However, the eddy currents on the boundary of the superconducting region cancel the applied field, and the condition $\boldsymbol{B} = 0$ is met inside the superconductor. The flux through the region surrounded by the superconductor is

$$\Phi = \int_F \boldsymbol{B}\cdot\boldsymbol{n}\,\mathrm{d}S, \tag{26.4.27}$$

where the surface F can be chosen at will, with the sole restriction that its contour should be inside the superconducting region, and $\boldsymbol{n}$ is the unit normal of the surface element. By expressing the magnetic induction in terms of the vector potential and using Stokes' theorem, the surface integral can be transformed into the integral around the contour C:

$$\Phi = \int_C \boldsymbol{A} \cdot \mathrm{d}\boldsymbol{l} \,. \tag{26.4.28}$$

$\boldsymbol{A}$ can be expressed from the second Ginzburg–Landau equation as

$$\boldsymbol{A} = -\frac{m^*}{e^{*2}} \frac{1}{|\psi|^2} \boldsymbol{j} - \frac{\hbar}{2\mathrm{i}e^*} \frac{1}{|\psi|^2} \left(\psi^* \boldsymbol{\nabla}\psi - \psi \boldsymbol{\nabla}\psi^*\right) . \tag{26.4.29}$$

Sufficiently far from the surface, where no diamagnetic current flows and the superconducting order is established, the magnitude of the order parameter ψ is given by the equilibrium value but its phase may still change. Assuming that it can be written as $\psi = |\psi_0| \mathrm{e}^{\mathrm{i}\phi}$,

$$\boldsymbol{A} = -\frac{\hbar}{e^*} \boldsymbol{\nabla}\phi \,. \tag{26.4.30}$$

Using this form of $\boldsymbol{A}$ in the integral around the contour C, which is chosen in such a way that the current should vanish along it, we have

$$\Phi = -\frac{\hbar}{e^*} \int_C \boldsymbol{\nabla}\phi \, \mathrm{d}\boldsymbol{l} \,. \tag{26.4.31}$$

The absolute value of the order parameter ψ is a single-valued function of the position but the phase is not. A full turn around the normal region may change the phase by an integral multiple of 2π. Therefore the flux enclosed by the contour C is

$$\Phi = n \, 2\pi \frac{\hbar}{e^*} = n \frac{h}{e^*} \,. \tag{26.4.32}$$

Since $e^* = 2e$, the elementary flux quantum is

$$\Phi_0 = \frac{h}{2e} = 2.067 \times 10^{-15} \,\mathrm{Wb} = 2.067 \times 10^{-7} \,\mathrm{G\,cm^2} \,. \tag{26.4.33}$$

F. London discussed flux quantization in already 1950, but he made the assumption $e^* = e$, and so his result for the flux quantum was twice as large as the correct value. The correctness of the above formula was later confirmed by the experiments shown in Fig. 26.6.

If the contour C is chosen in such a way that current can flow around it then it is the fluxoid

$$\Phi' = \Phi + \mu_0 \lambda_\mathrm{L}^2 \int_C \boldsymbol{j}_\mathrm{s} \, \mathrm{d}\boldsymbol{l} \,, \tag{26.4.34}$$

rather than the flux, that is quantized, in units of Φ_0. As mentioned in connection with the London theory, this corresponds to the Bohr–Sommerfeld quantization of the canonical momentum.

26.4.5 Energy of the Normal Metal–Superconductor Interface

To understand when normal regions can be formed inside a superconductor, the energy of the interface between a superconductor and a normal metal has to be studied. This energy depends on the relative magnitude of the coherence length and the penetration depth. Two extreme cases are shown in Fig. 26.21.

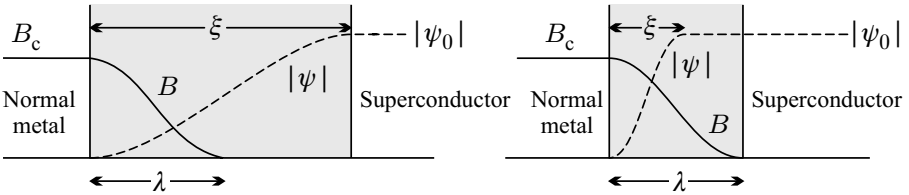

Fig. 26.21. The spatial variation of the magnetic induction and the superconducting order parameter at a normal metal–superconductor interface, in the $\lambda \ll \xi$ and $\lambda \gg \xi$ limits

The ratio $\kappa = \lambda/\xi$ of the penetration depth and coherence length, called the Ginzburg–Landau parameter, is a fundamental parameter of superconductors. When $\kappa \ll 1$, the magnetic field drops off much more rapidly than ψ grows up to its equilibrium value. There is a wide region where both $\boldsymbol{B}$ and ψ are small, i.e., both the superconducting condensate and the magnetic induction, which could reduce the energy, are absent. The surface energy of such a normal–superconductor interface is expected to be positive, so such walls are not formed spontaneously. The situation is the opposite in the $\kappa \gg 1$ case: the surface energy is expected to be negative, thus such walls are formed spontaneously. Below we shall give a better estimate for the surface energy.

When the applied magnetic field is considered as a free variable, the density of the Gibbs potential,

$$g = f - \boldsymbol{H} \cdot \boldsymbol{B}\,, \tag{26.4.35}$$

has to be minimized. Using the Ginzburg–Landau form (26.4.1) for the Helmholtz free energy, the Gibbs potential in given by

$$\begin{aligned} g_{\mathrm{n}}(T,H) &= f_{\mathrm{n}}(T,0) + \frac{1}{2\mu_0}\boldsymbol{B}^2 - \boldsymbol{H}\cdot\boldsymbol{B} \\ &= f_{\mathrm{n}}(T,0) - \tfrac{1}{2}\mu_0 H^2 \end{aligned} \tag{26.4.36}$$

in the normal state where the order parameter vanishes and $\boldsymbol{B} = \mu_0 \boldsymbol{H}$, while it is

$$\begin{aligned} g_{\mathrm{s}}(T,H) = f_n(T,0) &+ \alpha(T)|\psi|^2 + \tfrac{1}{2}\beta(T)|\psi|^4 \\ &+ \frac{1}{2m^*}\left|\left(\frac{\hbar}{\mathrm{i}}\boldsymbol{\nabla} + e^*\boldsymbol{A}\right)\psi\right|^2 + \frac{1}{2\mu_0}\boldsymbol{B}^2 - \boldsymbol{H}\cdot\boldsymbol{B} \end{aligned} \tag{26.4.37}$$

in the superconducting state.

When the applied magnetic field is equal to the thermodynamic critical field defined by

$$f_{\mathrm{s}}(T,0) = f_{\mathrm{n}}(T,0) - \tfrac{1}{2}\mu_0 H_{\mathrm{c}}^2\,, \tag{26.4.38}$$

then, according to (26.3.13), the Gibbs potential of the homogeneous superconductor is the same as that of the homogeneous normal phase. Their densities are given by

$$g_{\mathrm{s}}^{\mathrm{hom}}(T,H_{\mathrm{c}}) = g_{\mathrm{n}}^{\mathrm{hom}}(T,H_{\mathrm{c}}) = f_{\mathrm{n}}(T,0) - \tfrac{1}{2}\mu_0 H_{\mathrm{c}}^2\,. \tag{26.4.39}$$

When this common value – which is valid on both sides, at large distances from the interface – is subtracted from the actual density of the Gibbs potential calculated in the presence of an interface, and the difference is integrated in the direction perpendicular to the interface, the surface energy is found to be

$$\begin{aligned}\sigma_{\mathrm{ns}} &= \int_{-\infty}^{\infty} \left[g_{\mathrm{s}}(T,H_{\mathrm{c}}) - g_{\mathrm{n}}^{\mathrm{hom}}(T,H_{\mathrm{c}})\right] \mathrm{d}x \\ &= \int_{-\infty}^{\infty} \left\{\alpha(T)|\psi|^2 + \tfrac{1}{2}\beta(T)|\psi|^4 + \frac{1}{2m^*}\left|\left(\frac{\hbar}{\mathrm{i}}\boldsymbol{\nabla} + e^*\boldsymbol{A}\right)\psi\right|^2 \right. \\ &\qquad \left. + \frac{1}{2\mu_0}(B-\mu_0 H_{\mathrm{c}})^2\right\} \mathrm{d}x\,.\end{aligned} \tag{26.4.40}$$

By multiplying the first Ginzburg–Landau equation by ψ^*, and taking its integral along the x-axis, integration by parts yields

$$\int_{-\infty}^{\infty} \left\{\alpha(T)|\psi|^2 + \beta(T)|\psi|^4 + \frac{1}{2m^*}\left|\left(\frac{\hbar}{\mathrm{i}}\boldsymbol{\nabla} + e^*\boldsymbol{A}\right)\psi\right|^2\right\} \mathrm{d}x = 0\,. \tag{26.4.41}$$

Comparison with the previous equation gives the surface energy as

$$\sigma_{\mathrm{ns}} = \int_{-\infty}^{\infty} \left\{-\frac{1}{2}\beta(T)|\psi|^4 + \frac{(B-\mu_0 H_{\mathrm{c}})^2}{2\mu_0}\right\} \mathrm{d}x\,. \tag{26.4.42}$$

The role of ψ and B in determining the surface energy is clear. In the $\xi \gg \lambda$ limit B and ψ are small in the transition region of width ξ, so the free energy per unit surface area is

$$\sigma_{\mathrm{ns}} \approx \tfrac{1}{2}\xi\mu_0 H_{\mathrm{c}}^2\,, \tag{26.4.43}$$

which is indeed positive. In the opposite limit, $\lambda \gg \xi$, the wavefunction almost takes the equilibrium value over a large part of the transition region of width λ, however, the magnetic induction does not drop to zero, and so

$$\sigma_{\mathrm{ns}} \approx -\tfrac{1}{2}\lambda\mu_0 H_{\mathrm{c}}^2\,, \tag{26.4.44}$$

which means that the wall energy is negative.

In general, the wall energy can be determined only numerically. The special case $\kappa = 1/\sqrt{2}$ is an exception, since the Ginzburg–Landau equations then imply

$$|\psi|^2 = \frac{\mu_0 H_c - B}{(\mu_0 \beta)^{1/2}}\,, \tag{26.4.45}$$

that is, the integrand vanishes identically, and so the surface energy is zero. For $\kappa < 1/\sqrt{2}$ the surface energy is positive, thus the formation of walls is not advantageous energetically. Conversely, the surface energy is negative for $\kappa > 1/\sqrt{2}$, so the energy is lower when the system is made up of alternate normal and superconducting regions. The first case is realized in type I superconductors, and the second in type II superconductors.

26.4.6 Vortices

Type II superconductors in a thermodynamic critical field (or more generally, between the upper and lower critical fields) are thus not homogeneous, as the free energy of the system is lower if normal and superconducting regions alternate. To understand what happens in the superconducting phase in this geometry, we have to find a more accurate solution of the Ginzburg–Landau equations. As pointed out by A. A. Abrikosov[15] in 1957, the magnetic field penetrates into the superconductor in long tubes called *vortices*. This can be studied analytically for $\kappa \gg 1$, when $|\psi(\boldsymbol{r})|$ takes the asymptotic value everywhere except for a small core region. The dependence of the magnetic induction and superconducting order parameter on the distance from the center of the vortex are shown in Fig. 26.22.

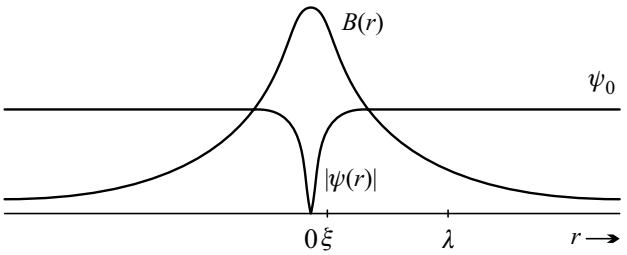

Fig. 26.22. The spatial variations of the magnetic induction and superconducting order parameter around a vortex core

(26.4.30), which was derived from the second Ginzburg–Landau equation, can be rewritten as

$$\boldsymbol{A} + \mu_0 \lambda_L^2 \boldsymbol{j} = -\frac{1}{2\pi} \Phi_0 \boldsymbol{\nabla} \phi\,. \tag{26.4.46}$$

[15] See the footnotes on pages 4 of Volume 1 and 483.

By taking an arbitrary contour that does not approach the vortex core within the coherence length ξ, and expressing the current in terms of the magnetic induction through the Maxwell equations, we have

$$\int_C \left(\boldsymbol{A} + \lambda_{\mathrm{L}}^2 \operatorname{curl} \boldsymbol{B}\right) \mathrm{d}\boldsymbol{l} = n\,\Phi_0\,. \tag{26.4.47}$$

The line integral on the left-hand side can be transformed into a surface integral by means of Stokes' theorem, yielding

$$\int_F \left(\operatorname{curl} \boldsymbol{A} + \lambda_{\mathrm{L}}^2 \operatorname{curl}\operatorname{curl} \boldsymbol{B}\right) \cdot \mathrm{d}\boldsymbol{S} = n\,\Phi_0\,. \tag{26.4.48}$$

When several vortices are present in a type II superconductor, each vortex carries exactly one flux quantum in the energetically most favorable configuration. As $\xi \ll \lambda_{\mathrm{L}}$, we shall study the structure of the vortex in the $\xi \to 0$ limit. The previous equation is satisfied by an arbitrary contour if

$$\boldsymbol{B} + \lambda_{\mathrm{L}}^2 \operatorname{curl}\operatorname{curl} \boldsymbol{B} = \hat{\boldsymbol{z}}\Phi_0\delta_2(\boldsymbol{r})\,, \tag{26.4.49}$$

where $\delta_2(\boldsymbol{r})$ is a δ function in the perpendicular plane, and $\hat{\boldsymbol{z}}$ is the unit vector in the direction of the magnetic field.

Compared to the London equation, an additional source term has appeared. Since $\operatorname{div} \boldsymbol{B} = 0$,

$$\boldsymbol{B} - \lambda_{\mathrm{L}}^2 \boldsymbol{\nabla}^2 \boldsymbol{B} = \Phi_0 \hat{\boldsymbol{z}} \delta_2(\boldsymbol{r})\,. \tag{26.4.50}$$

Changing to cylindrical coordinates, and assuming that $\boldsymbol{B}$ has only one nonvanishing component, B_z, which depends only on r, we have

$$B_z - \frac{\lambda_{\mathrm{L}}^2}{r} \frac{\mathrm{d}}{\mathrm{d}r} \left(r \frac{\mathrm{d}B_z}{\mathrm{d}r} \right) = \Phi_0 \delta_2(\boldsymbol{r})\,. \tag{26.4.51}$$

Outside the vortex core the solution is

$$B_z(r) = \frac{\Phi_0}{2\pi\lambda_{\mathrm{L}}^2} K_0 \left(\frac{r}{\lambda_{\mathrm{L}}} \right), \tag{26.4.52}$$

where K_0 is the zeroth-order modified Bessel function, while inside the vortex

$$B_z(r) = \frac{\Phi_0}{2\pi\lambda_{\mathrm{L}}^2} K_0 \left(\frac{\xi}{\lambda_{\mathrm{L}}} \right). \tag{26.4.53}$$

Using the form given in (C.3.59), simple analytic formulas are obtained in two limits:

$$B_z(r) = \begin{cases} \dfrac{\Phi_0}{2\pi\lambda_{\mathrm{L}}^2} \left(\dfrac{\pi\lambda_{\mathrm{L}}}{2r} \right)^{1/2} \mathrm{e}^{-r/\lambda_{\mathrm{L}}}, & \text{if} \quad r \to \infty\,, \\ \dfrac{\Phi_0}{2\pi\lambda_{\mathrm{L}}^2} \left(\ln \dfrac{\lambda_{\mathrm{L}}}{r} + 0.12 \right), & \text{if} \quad \xi \ll r \ll \lambda_{\mathrm{L}}\,. \end{cases} \tag{26.4.54}$$

Note that over the largest part of the Shubnikov phase the separation of vortices is smaller than the penetration depth, thus the magnetic induction is finite everywhere in the sample.

The radial variation of the current circulating around the vortex core is given by

$$j(r) = -\frac{\Phi_0}{2\pi\lambda_\mathrm{L}^3\mu_0} K_1\left(\frac{r}{\lambda_\mathrm{L}}\right) \tag{26.4.55}$$

outside the core. Far from the core of an isolated vortex, $j(r)$ decays exponentially, too, however it decreases as $1/r$ in the region $\xi \ll r \ll \lambda_\mathrm{L}$. Determined from the spatial dependence, the vortex energy per unit length is

$$E_\mathrm{vortex} = \frac{\Phi_0^2}{4\pi\mu_0\lambda_\mathrm{L}^2} \ln\left(\frac{\lambda_\mathrm{L}}{\xi}\right). \tag{26.4.56}$$

This result could have been found intuitively. Since the current of superconducting electrons is cylindrically symmetric around the vortex core, the associated velocity can be determined from the quantization condition

$$\oint \boldsymbol{p} \cdot \mathrm{d}\boldsymbol{l} = nh \tag{26.4.57}$$

for the canonical momentum $\boldsymbol{p}$ if the latter is approximated by the kinetic momentum $m^*\boldsymbol{v}_\mathrm{s}$. Taken around a circle of radius r, the integral is

$$nh = m^* \oint \boldsymbol{v}_\mathrm{s} \cdot \mathrm{d}\boldsymbol{l} = m^* v_\mathrm{s} 2\pi r\,, \tag{26.4.58}$$

and hence

$$v_\mathrm{s} = \frac{n\hbar}{m^* r}\,. \tag{26.4.59}$$

It can be assumed that the dominant part of the circulating current flows in a region into which the field can penetrate and where the order parameter has almost reached its equilibrium value – that is, where the distances r from the vortex core is larger than the coherence length ξ but smaller than the penetration depth λ_L. When the $n = 1$ solution is applied to each vortex, the kinetic energy of the superconducting electrons in a layer of unit height around the vortex core is

$$E_\mathrm{kin} = n_\mathrm{s}^* \int_\xi^{\lambda_\mathrm{L}} \frac{m^* v_\mathrm{s}^2}{2}\, 2\pi r\, \mathrm{d}r = \frac{\pi n_\mathrm{s}^* \hbar^2}{m^*} \int_\xi^{\lambda_\mathrm{L}} \frac{\mathrm{d}r}{r} = \frac{\pi n_\mathrm{s}^* \hbar^2}{m^*} \ln\kappa\,. \tag{26.4.60}$$

Using the formulas of the flux quantum and the London penetration depth, the vortex energy obtained in (26.4.56) is indeed recovered.

It can be shown that when two vortices are located at $\boldsymbol{r}_1$ and $\boldsymbol{r}_2$, separated by a distance r_{12}, their interaction energy is

$$E_{12} = \frac{\Phi_0^2}{2\pi\mu_0\lambda^2} K_0\left(\frac{r_{12}}{\lambda_\mathrm{L}}\right), \tag{26.4.61}$$

that is, the interaction decays exponentially at large distances. This result lends itself to simple interpretation in terms of the magnetic moment of the vortex. The angular momentum due to the circulating current is

$$\hbar L = n_\mathrm{s}^* \int_\xi^{\lambda_\mathrm{L}} r m^* v_\mathrm{s} 2\pi r \,\mathrm{d}r = n_\mathrm{s}^* \pi\hbar\lambda_\mathrm{L}^2 \,. \tag{26.4.62}$$

The magnetic moment is obtained by multiplying it by $e^*/2m^*$:

$$\mu = \frac{\pi n_\mathrm{s}^* e^* \hbar}{2m^*} \lambda_\mathrm{L}^2 = \frac{\Phi_0}{4\mu_0} \,. \tag{26.4.63}$$

When such a magnetic moment is placed into the field $B(r_{12})$ of the other vortex, the same interaction energy is found as above.

Since the interaction between vortices is repulsive, the lowest-energy configuration for a given flux is obtained by separating the vortices as much as possible. This is realized in periodic structures. Two possibilities are shown in Fig. 26.23: a square and a triangular lattice.

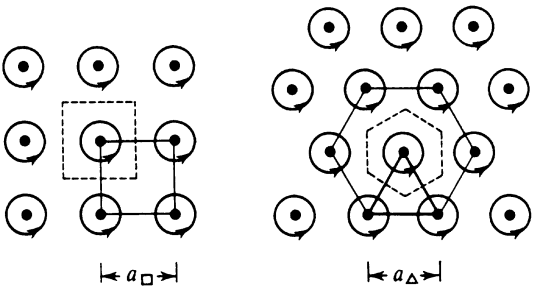

Fig. 26.23. Vortex arrangement in two-dimensional square and triangular lattices

Simple considerations show that the triangular vortex lattice in energetically more favorable. If the flux through the surface area F of the sample is $BF = \Phi = n\Phi_0$, and each vortex carries a flux quantum, then the lattice constant $a_\square$ of the square vortex lattice is given by

$$a_\square^2 B = \Phi_0 \,, \qquad a_\square = \left(\frac{\Phi_0}{B}\right)^{1/2} , \tag{26.4.64}$$

whereas for a triangular lattice

$$a_{\triangle}\frac{\sqrt{3}}{2}a_{\triangle}B = \Phi_0\,, \qquad a_{\triangle} = \left(\frac{4}{3}\right)^{1/4}\left(\frac{\Phi_0}{B}\right)^{1/2} = 1.075\left(\frac{\Phi_0}{B}\right)^{1/2}, \tag{26.4.65}$$

so for a given flux $a_{\triangle} > a_{\square}$. The arrangement of vortices in such a triangular lattice is indeed observed in conventional superconductors. The image in Fig. 26.24, taken by a scanning tunneling microscope, shows the surface of a type II superconductor in the Shubnikov phase.

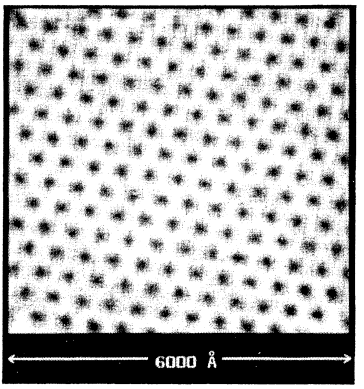

Fig. 26.24. The STM image of the vortex lattice observed in a $NbSe_2$ sample in a magnetic field of 1 T at a temperature of 1.8 K [Reprinted with permission from H. F. Hess et al., *Phys. Rev. Lett.* **62**, 214 (1989). ©1989 by the American Physical Society]

The situation is slightly different in high-T_c superconductors. When the sample is heated in an applied magnetic field H that is somewhat above the lower critical field $H_{c1}(T)$, the vortex lattice may melt before reaching the relatively high critical temperature for this field, and thus a vortex liquid can appear. It has not been confirmed by experiments whether the vortices really make up a lattice before making a transition to the liquid-like state in fields above $H_{c1}(T)$ or are disordered at lower temperatures, too. Theoretical considerations support the assumption that a statically disordered, glass-like *vortex-glass* state is realized. The corresponding phase diagram is shown in Fig. 26.25.

26.4.7 Upper and Lower Critical Fields

In the foregoing the necessity of the appearance of vortices (i.e., alternating normal and superconducting regions) was demonstrated theoretically for type II superconductors placed in the thermodynamic critical field. However, it is known from experiments that in conventional superconductors the inhomogeneous Shubnikov phase with vortices is stable for fields between the lower and upper critical fields, H_{c1} and H_{c2}. Below H_{c1}, type II superconductors are

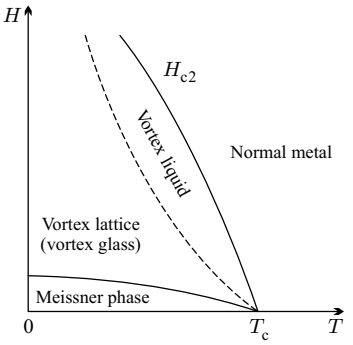

Fig. 26.25. Schematic phase diagram of high-T_c superconductors

also perfect diamagnets, fully displaying the Meissner–Ochsenfeld effect, while they make a transition into the normal state above H_{c2}. Using the previous result, we can now determine the values of the two critical fields.

For fields close to H_{c1}, where the magnetization is small, the separation of vortices becomes so large that their interaction can be neglected. Whether or not a vortex can appear is determined by the relative strength of the two competing terms in the Gibbs potential. According to (26.4.56), the vortex itself has a positive energy. In a sample of length L, the energy of the vortex is LE_{vortex}. This can be compensated by the magnetic field contribution $-\boldsymbol{B}\cdot\boldsymbol{H}$ in the Gibbs potential. Assuming that the magnetic flux through the vortex is exactly one flux quantum, the integral of the magnetic field contribution over the volume of the sample is

$$-\int\limits_V \boldsymbol{B}\cdot\boldsymbol{H}\,\mathrm{d}V = -L\,H\int\limits_F \boldsymbol{B}\cdot\mathrm{d}\boldsymbol{S} = -L\,H\Phi_0\,. \tag{26.4.66}$$

The first vortex may appear at that value H_{c1} of the field where the two contributions are equal:

$$H_{c1}\Phi_0 = E_{\text{vortex}}\,. \tag{26.4.67}$$

Using the vortex-energy formula, the lower critical field is

$$H_{c1} = \frac{\Phi_0}{4\pi\mu_0\lambda_L^2}\ln\kappa\,. \tag{26.4.68}$$

In slightly stronger fields the sudden appearance of a large number of vortices is prevented by the repulsive interaction between vortices. Therefore the number of vortices increases step by step, while their separation is still larger than λ, and the magnetic field penetrates into the sample gradually.

Now consider what happens in strong magnetic fields, when the mixed state is transformed into normal metal. Assuming that the order parameter is small in the vicinity of the transition point, the first Ginzburg–Landau equation can be linearized:

$$\frac{1}{2m^*}\left(\frac{\hbar}{\mathrm{i}}\boldsymbol{\nabla}+e^*\boldsymbol{A}\right)^2\psi=-\alpha\psi\,. \tag{26.4.69}$$

Formally, this is the same Schrödinger equation as (22.1.13), from which the energy levels (Landau levels) of a noninteracting electron gas placed in a strong magnetic field were determined. Adopting the results obtained there to the present case, the energy eigenvalues are

$$\varepsilon=\frac{\hbar^2k_z^2}{2m^*}+(n+\tfrac{1}{2})\hbar\omega_{\mathrm{c}}^*\,, \tag{26.4.70}$$

where, on account of $e^*=2e$,

$$\hbar\omega_{\mathrm{c}}^*=\hbar\frac{e^*B}{m^*}=\hbar\frac{2eB}{m^*}\,. \tag{26.4.71}$$

In (26.4.69) $-\alpha$ plays the role of the energy eigenvalue. At temperatures below T_{c}, where α is negative, the superconducting order parameter ψ is nonzero if $-\alpha$ is equal to one of the eigenvalues in (26.4.70). The strongest magnetic field for which the condition

$$-\alpha\geq\varepsilon_{\min}=\tfrac{1}{2}\hbar\omega_{\mathrm{c}}^*=\hbar\frac{eB}{m^*} \tag{26.4.72}$$

can be satisfied – and therefore a superconducting state may exist – is then given by

$$H_{\mathrm{c}2}=-\alpha\frac{m^*}{e\hbar\mu_0}\,. \tag{26.4.73}$$

The parameter α of the Ginzburg–Landau theory can be related to the coherence length ξ through (26.4.15). Making use of this connection,

$$H_{\mathrm{c}2}=\frac{\hbar}{2e\mu_0\xi^2}=\frac{\Phi_0}{2\pi\mu_0\xi^2}\,. \tag{26.4.74}$$

Close to $H_{\mathrm{c}2}$, vortices are present in a relatively high number. The previous formula can be interpreted by saying that superconductivity is destroyed at that value of the magnetic field where the separation of vortices becomes comparable to the coherence length.

When a Ginzburg–Landau-like phenomenological description is applied to anisotropic superconductors, it is quite natural to assume that an effective-mass tensor can be used in the term that contains the gradient of the order parameter. Instead of (26.4.69), the linearization of the first Ginzburg-Landau equation then leads to

$$\frac{1}{2}\sum_{\alpha\beta}\left(\frac{\hbar}{\mathrm{i}}\boldsymbol{\nabla}+e^*\boldsymbol{A}\right)_\alpha\left(\frac{1}{m^*}\right)_{\alpha\beta}\left(\frac{\hbar}{\mathrm{i}}\boldsymbol{\nabla}+e^*\boldsymbol{A}\right)_\beta\psi=-\alpha\psi\,. \tag{26.4.75}$$

Once again, this is a Schrödinger equation for the one-particle spectrum of an electron gas in a strong magnetic field, but the spectrum in zero magnetic

field is now characterized by an effective-mass tensor. The energy of the Landau levels can again be written as (26.4.70) but now the motion in the field direction and the cyclotron frequency are determined by the components of the effective-mass tensor, in combinations that depend on the field direction. Thus the upper critical field is obtained from (26.4.72) here, too. Assuming that there are one longitudinal and two identical transverse masses, $m^*_\parallel$ and $m^*_\perp$, when the magnetic field makes an angle θ with the longitudinal direction, and the cyclotron mass in ω^*_c is taken from (21.2.42), we have

$$\omega^*_\mathrm{c} = 2eB \left(\frac{\sin^2\theta}{m^*_\parallel m^*_\perp} + \frac{\cos^2\theta}{(m^*_\perp)^2} \right)^{1/2} , \tag{26.4.76}$$

where the factor 2 comes from the double charge of the Cooper pairs. When the magnetic field is parallel or perpendicular to the symmetry axis, the upper critical field can be written as

$$H_{\mathrm{c}2\parallel} = \frac{\Phi_0}{2\pi\mu_0 \xi_\parallel \xi_\perp} , \qquad H_{\mathrm{c}2\perp} = \frac{\Phi_0}{2\pi\mu_0 \xi^2_\perp} , \tag{26.4.77}$$

where

$$\xi^2_\parallel = \frac{\hbar^2}{2m^*_\parallel a(T_\mathrm{c} - T)} , \qquad \xi^2_\perp = \frac{\hbar^2}{2m^*_\perp a(T_\mathrm{c} - T)} . \tag{26.4.78}$$

In the isotropic case the upper and lower critical fields can also be expressed in terms of the thermodynamic critical field. It is known from Landau's theory of phase transitions that the free energy decreases by $\alpha^2/2\beta$ in the ordered phase. On the other hand, the thermodynamic critical field is defined precisely by the equality of the free energy in the superconducting and normal phases. This leads to

$$\tfrac{1}{2}\mu_0 H^2_\mathrm{c} = \frac{\alpha^2}{2\beta} . \tag{26.4.79}$$

Using the previously obtained formulas for the London penetration depth and coherence length,

$$H_\mathrm{c} = \frac{\Phi_0}{2\sqrt{2}\pi\mu_0 \lambda_\mathrm{L} \xi} . \tag{26.4.80}$$

Thus

$$H_{\mathrm{c}1} = \frac{1}{\sqrt{2}} \frac{1}{\kappa} H_\mathrm{c} \ln\kappa , \qquad H_{\mathrm{c}2} = \sqrt{2}\,\kappa\, H_\mathrm{c} . \tag{26.4.81}$$

In type II superconductors, where $\kappa > 1/\sqrt{2}$, $H_{\mathrm{c}1} < H_\mathrm{c} < H_{\mathrm{c}2}$. As the applied field is increased, the Meissner phase becomes unstable below the thermodynamic critical field, and the new phase remains stable even at fields that are stronger than the thermodynamic critical field. This is possible because of the nonuniformity of the superconducting order parameter. In type I superconductors, where the upper critical field $H_{\mathrm{c}2}$ is smaller than H_c, the homogeneous superconducting order disappears and reappears at H_c as the field strength

is increased and decreased. It is nevertheless possible to attribute a physical meaning to H_{c2}. Since in type I superconductors the phase transition at finite temperatures and finite magnetic fields is first order, the normal phase can be "supercooled", as shown in Fig. 26.7. H_{c2} specifies the lowest field for which the normal phase can exist when the applied magnetic field is reduced.

It is worth noting that a similar hysteresis can be observed in type II superconductors, too, at H_{c1}. The reason for this is that when field lines penetrate into the superconductor in the form of a vortex, a potential barrier has to be surmounted. The force on a vortex appearing inside the sample, close to the surface, can be described as an attraction between the vortex and its "mirror image" of opposite vorticity that is outside the sample.

26.5 Josephson Effect

It has already been mentioned that when superconducting material is placed on one or both sides of a junction, the current–voltage characteristics are not linear. This current comes from the tunneling of normal electrons, which can only be present in the system at energies above the gap. That is why the gap can be determined from the I–V characteristics. In 1962 B. D. Josephson[16] recognized that if superconductors are placed on both sides of the junction, superconducting electrons can also tunnel through the junction. We shall discuss this effect now.

26.5.1 Relation Between the Josephson Current and the Phase of the Superconductor

In order to draw a simple picture of the Josephson effect, we suppose that the width d of the insulating layer of the junction is much smaller than the coherence length: $d \ll \xi$. In line with the Ginzburg–Landau theory we assume that the system can be characterized by a complex function ψ that takes its equilibrium value far from the insulating layer, but with different phases ϕ_{L} and ϕ_{R} on the two sides. If two identical superconductors fill the regions $x < -d/2$ and $x > d/2$,

$$\psi(x) = \begin{cases} |\psi_0| \mathrm{e}^{\mathrm{i}\phi_{\mathrm{L}}} & x < -d/2\,, \\ |\psi_0| \mathrm{e}^{\mathrm{i}\phi_{\mathrm{R}}} & x > d/2\,. \end{cases} \tag{26.5.1}$$

The spatial variation in the insulating layer can be determined from the first Ginzburg–Landau equation. In the zero-field case the equation (26.4.20) for

[16] Brian David Josephson (1940–) was awarded the Nobel Prize in 1973 "for his theoretical predictions of the properties of a supercurrent through a tunnel barrier, in particular those phenomena which are generally known as the Josephson effects".

$f = \psi/|\psi_0|$ has to be considered. Based on the geometry of the system, we assume that the characteristic scale for the spatial variations of the order parameter is the thickness of the insulating layer. Then, on account of the huge factor $(\xi/d)^2$ that appears on the left-hand side, the equation can be satisfied only if $\mathrm{d}^2 f/\mathrm{d}x^2 = 0$. The requirement that the solution should match smoothly at the boundary of the insulating layer with the value in the superconductors leads to

$$f(x) \approx \left(\frac{1}{2} - \frac{x}{d}\right) \mathrm{e}^{\mathrm{i}\phi_\mathrm{L}} + \left(\frac{1}{2} + \frac{x}{d}\right) \mathrm{e}^{\mathrm{i}\phi_\mathrm{R}} \qquad -d/2 \le x \le d/2\,. \tag{26.5.2}$$

The spatial variation of the order parameter over the Josephson junction is shown in Fig. 26.26.

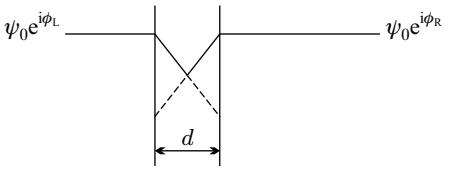

Fig. 26.26. Variation of the real part of the order parameter in a Josephson junction

The current determined from this wavefunction by means of the second Ginzburg–Landau equation is

$$j = \frac{2e\hbar|\psi_0|^2}{m^* d} \sin(\phi_\mathrm{R} - \phi_\mathrm{L})\,, \tag{26.5.3}$$

that is, the supercurrent through the junction depends on the difference of the macroscopic phases of the superconductors on each side.

For the sake of later generalization, it is worth giving a brief overview of two more accurate methods. In the first approach, developed by Feynman,[17] the superconductors – which are not necessarily identical – on the two sides of the junction are each described in terms of a complex order parameter, the wavefunction of the superconducting electrons,

$$\psi_\mathrm{L} = |\psi_\mathrm{L}|\mathrm{e}^{\mathrm{i}\phi_\mathrm{L}}\,, \qquad \psi_\mathrm{R} = |\psi_\mathrm{R}|\mathrm{e}^{\mathrm{i}\phi_\mathrm{R}}\,, \tag{26.5.4}$$

just like in the Ginzburg–Landau theory. In an isolated superconductor the time dependence of the wavefunction is determined by the chemical potential, as ψ satisfies the time-dependent Schrödinger equation

$$-\frac{\hbar}{\mathrm{i}}\frac{\partial\psi}{\partial t} = \mu\psi\,. \tag{26.5.5}$$

[17] R. P. Feynman, 1965. See also the footnote on page 532 of Volume 1.

Because of the tunnel coupling in the Josephson junction, the wavefunction of the other side also appears in the equations. The coupling between the two sides can be taken into account by a phenomenological coupling constant T as

$$\begin{aligned} -\frac{\hbar}{\mathrm{i}}\frac{\partial\psi_{\mathrm{L}}}{\partial t} &= \mu_{\mathrm{L}}\psi_{\mathrm{L}} + T\psi_{\mathrm{R}}\,, \\ -\frac{\hbar}{\mathrm{i}}\frac{\partial\psi_{\mathrm{R}}}{\partial t} &= \mu_{\mathrm{R}}\psi_{\mathrm{R}} + T\psi_{\mathrm{L}}\,. \end{aligned} \tag{26.5.6}$$

Substitution of the formulas in (26.5.4) leads to

$$\begin{aligned} \frac{\partial|\psi_{\mathrm{L}}|}{\partial t}\mathrm{e}^{\mathrm{i}\phi_{\mathrm{L}}} + \mathrm{i}|\psi_{\mathrm{L}}|\mathrm{e}^{\mathrm{i}\phi_{\mathrm{L}}}\frac{\partial\phi_{\mathrm{L}}}{\partial t} &= -\frac{\mathrm{i}}{\hbar}\mu_{\mathrm{L}}|\psi_{\mathrm{L}}|\mathrm{e}^{\mathrm{i}\phi_{\mathrm{L}}} - \frac{\mathrm{i}}{\hbar}T|\psi_{\mathrm{R}}|\mathrm{e}^{\mathrm{i}\phi_{\mathrm{R}}}, \\ \frac{\partial|\psi_{\mathrm{R}}|}{\partial t}\mathrm{e}^{\mathrm{i}\phi_{\mathrm{R}}} + \mathrm{i}|\psi_{\mathrm{R}}|\mathrm{e}^{\mathrm{i}\phi_{\mathrm{R}}}\frac{\partial\phi_{\mathrm{R}}}{\partial t} &= -\frac{\mathrm{i}}{\hbar}\mu_{\mathrm{R}}|\psi_{\mathrm{R}}|\mathrm{e}^{\mathrm{i}\phi_{\mathrm{R}}} - \frac{\mathrm{i}}{\hbar}T|\psi_{\mathrm{L}}|\mathrm{e}^{\mathrm{i}\phi_{\mathrm{L}}}. \end{aligned} \tag{26.5.7}$$

After some algebra we obtain

$$\begin{aligned} \frac{\partial|\psi_{\mathrm{L}}|}{\partial t} + \mathrm{i}|\psi_{\mathrm{L}}|\frac{\partial\phi_{\mathrm{L}}}{\partial t} &= -\frac{\mathrm{i}}{\hbar}\mu_{\mathrm{L}}|\psi_{\mathrm{L}}| - \frac{\mathrm{i}}{\hbar}T|\psi_{\mathrm{R}}|\mathrm{e}^{\mathrm{i}(\phi_{\mathrm{R}}-\phi_{\mathrm{L}})}, \\ \frac{\partial|\psi_{\mathrm{R}}|}{\partial t} + \mathrm{i}|\psi_{\mathrm{R}}|\frac{\partial\phi_{\mathrm{R}}}{\partial t} &= -\frac{\mathrm{i}}{\hbar}\mu_{\mathrm{R}}|\psi_{\mathrm{R}}| - \frac{\mathrm{i}}{\hbar}T|\psi_{\mathrm{L}}|\mathrm{e}^{-\mathrm{i}(\phi_{\mathrm{R}}-\phi_{\mathrm{L}})}. \end{aligned} \tag{26.5.8}$$

By separating the real and imaginary parts,

$$\begin{aligned} \frac{\partial|\psi_{\mathrm{L}}|}{\partial t} &= \frac{1}{\hbar}T|\psi_{\mathrm{R}}|\sin(\phi_{\mathrm{R}}-\phi_{\mathrm{L}})\,, \\ \frac{\partial|\psi_{\mathrm{R}}|}{\partial t} &= -\frac{1}{\hbar}T|\psi_{\mathrm{L}}|\sin(\phi_{\mathrm{R}}-\phi_{\mathrm{L}})\,, \end{aligned} \tag{26.5.9}$$

and

$$\begin{aligned} \frac{\partial\phi_{\mathrm{L}}}{\partial t} &= -\frac{1}{\hbar}\mu_{\mathrm{L}} - \frac{1}{\hbar}T\frac{|\psi_{\mathrm{R}}|}{|\psi_{\mathrm{L}}|}\cos(\phi_{\mathrm{R}}-\phi_{\mathrm{L}})\,, \\ \frac{\partial\phi_{\mathrm{R}}}{\partial t} &= -\frac{1}{\hbar}\mu_{\mathrm{R}} - \frac{1}{\hbar}T\frac{|\psi_{\mathrm{L}}|}{|\psi_{\mathrm{R}}|}\cos(\phi_{\mathrm{R}}-\phi_{\mathrm{L}})\,. \end{aligned} \tag{26.5.10}$$

The real part is related to the variations of the amplitude – that is, the variations of the number of superconducting electrons. The current density carried by the particles of charge $-e^*$ is

$$j = -e^*\frac{\partial|\psi_{\mathrm{R}}|^2}{\partial t} = \frac{2e^*}{\hbar}T|\psi_{\mathrm{L}}||\psi_{\mathrm{R}}|\sin(\phi_{\mathrm{R}}-\phi_{\mathrm{L}})\,. \tag{26.5.11}$$

Thus, the supercurrent through the Josephson junction depends on the phase difference of the two superconductors, just as in the simple derivation.

Let us turn to the second method now. It was mentioned in connection with the Ginzburg–Landau equations that the usual boundary condition given by

(26.4.6) cannot be applied when current is allowed to flow through the interface. Assuming the most general Cauchy boundary condition, the values of the wavefunctions and their derivatives on the interface satisfy the simultaneous equations

$$\begin{aligned} \psi_{\mathrm{L}} &= \lambda_{11}\psi_{\mathrm{R}} + \lambda_{12}\left(\frac{\mathrm{d}}{\mathrm{d}x} + \frac{\mathrm{i}e^*}{\hbar}\boldsymbol{A}\right)\psi_{\mathrm{R}}\,, \\ \left(\frac{\mathrm{d}}{\mathrm{d}x} + \frac{\mathrm{i}e^*}{\hbar}\boldsymbol{A}\right)\psi_{\mathrm{L}} &= \lambda_{21}\psi_{\mathrm{R}} + \lambda_{22}\left(\frac{\mathrm{d}}{\mathrm{d}x} + \frac{\mathrm{i}e^*}{\hbar}\boldsymbol{A}\right)\psi_{\mathrm{R}}\,. \end{aligned} \tag{26.5.12}$$

As usual, the vector potential was added to the derivative to have gauge-invariant equations. Since the currents calculated from the left- and right-hand-side wavefunctions must be equal, the coefficients λ have to satisfy the auxiliary condition

$$\lambda_{11}\lambda_{22} - \lambda_{12}\lambda_{21} = 1\,. \tag{26.5.13}$$

Determined from the second Ginzburg–Landau equation, the current is then

$$\begin{aligned} j &= \frac{\mathrm{i}e^*\hbar}{2m^*}\psi_{\mathrm{R}}^*\left(\frac{\mathrm{d}}{\mathrm{d}x} + \frac{\mathrm{i}e^*}{\hbar}\boldsymbol{A}\right)\psi_{\mathrm{R}} + \text{c.c.} \\ &= \frac{\mathrm{i}e^*\hbar}{2m^*}\left\{\psi_{\mathrm{R}}^*\left[\frac{1}{\lambda_{12}}\psi_{\mathrm{L}} - \frac{\lambda_{11}}{\lambda_{12}}\psi_{\mathrm{R}}\right] - \psi_{\mathrm{R}}\left[\frac{1}{\lambda_{12}}\psi_{\mathrm{L}}^* - \frac{\lambda_{11}}{\lambda_{12}}\psi_{\mathrm{R}}^*\right]\right\} \\ &= \frac{\mathrm{i}e^*\hbar}{2m^*\lambda_{12}}\left[\psi_{\mathrm{R}}^*\psi_{\mathrm{L}} - \psi_{\mathrm{R}}\psi_{\mathrm{L}}^*\right] \\ &= \frac{e^*\hbar}{m^*\lambda_{12}}\left|\psi_{\mathrm{L}}\right|\left|\psi_{\mathrm{R}}\right|\sin\left(\phi_{\mathrm{R}} - \phi_{\mathrm{L}}\right), \end{aligned} \tag{26.5.14}$$

in agreement with the previous results.

Next, we have to examine how the phases of the superconductors on each side of the junction change with the applied voltage across or magnetic field at the tunnel junction.

26.5.2 DC Josephson Effect

An important result of Feynman's treatment is the establishment of the system of equations (26.5.10) for the variation of the phases with time. For identical superconductors, when $|\psi_{\mathrm{L}}| = |\psi_{\mathrm{R}}|$,

$$\frac{\partial\phi_{\mathrm{R}}}{\partial t} - \frac{\partial\phi_{\mathrm{L}}}{\partial t} = \frac{1}{\hbar}(\mu_{\mathrm{L}} - \mu_{\mathrm{R}})\,. \tag{26.5.15}$$

If there is no voltage across the junction, the chemical potential is the same on both sides. Then

$$\frac{\partial}{\partial t}(\phi_{\mathrm{R}} - \phi_{\mathrm{L}}) = 0\,, \tag{26.5.16}$$

so the phase difference is constant, and a constant supercurrent can flow through the junction. This is the *direct-current (DC) Josephson effect*.

By writing the Josephson current through the junction of cross-sectional area A as

$$I_{\mathrm{J}} = I_0 \sin(\phi_{\mathrm{R}} - \phi_{\mathrm{L}}) \,, \tag{26.5.17}$$

it can be shown on the basis of the microscopic theory that the maximum supercurrent that can be driven through the junction without any voltage drop is determined by the superconducting gap and the resistance R_{n} of the junction measured in its normal state. At $T = 0$

$$I_0(T = 0) = \frac{\pi \Delta}{2eR_{\mathrm{n}}} \,, \tag{26.5.18}$$

while at finite temperatures

$$I_0(T) = \frac{\pi \Delta}{2eR_{\mathrm{n}}} \tanh(\Delta / 2k_{\mathrm{B}}T) \,. \tag{26.5.19}$$

At the threshold voltage $V_{\mathrm{c}} = 2\Delta/e$, where normal current starts to flow, the value of the single-particle tunneling current is exactly the same as the maximum supercurrent. At higher voltages the current gradually reaches the value $I = V/R_{\mathrm{n}}$ that corresponds to ohmic behavior of the normal state. The current–voltage characteristic is shown in Fig. 26.27.

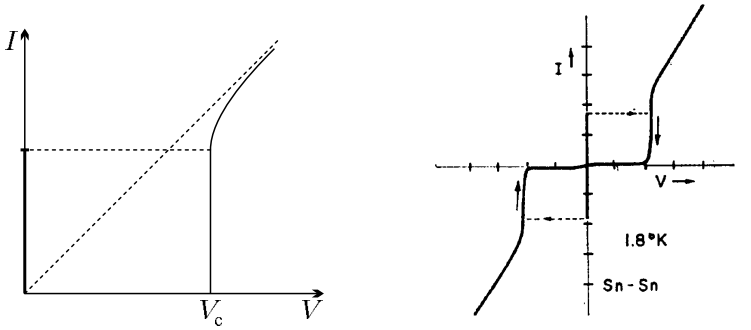

Fig. 26.27. *I–V* curve for a Josephson junction at zero temperature, and the measured supercurrent and single-particle current in an Sn-SnO_x-Sn junction at $T = 1.8\,\mathrm{K}$ [Reprinted with permission from R. C. Jaklevic et al., *Phys. Rev.* **140**, A 1628 (1965). ©1965 by the American Physical Society]

Experiments are in good agreement with the theoretical prediction that at low temperatures the maximum supercurrent that can be driven through the Josephson junction without any voltage drop is $\pi/4$ times the current that would flow through the junction in its normal state at the threshold voltage V_{c}. If a stronger current is passed through, a finite voltage V appears across the junction.

26.5.3 AC Josephson Effect

A voltage V applied between two superconductors gives rise to a chemical potential difference $-e^*V$ between the two sides. In the Josephson effect, where "superconducting electrons" of charge $-e^* = -2e$ tunnel, the formula

$$\mu_{\mathrm{R}} - \mu_{\mathrm{L}} = -e^*V = -2eV \tag{26.5.20}$$

has to be applied. The equation for the phase difference of the two superconductors, (26.5.15), now reads

$$\frac{\partial}{\partial t}(\phi_{\mathrm{R}} - \phi_{\mathrm{L}}) = 2\frac{eV}{\hbar}\,. \tag{26.5.21}$$

It can also be considered as the consequence of gauge invariance, as the gauge transformation (26.4.11) takes the scalar potential φ into

$$\varphi' = \varphi + \frac{\Phi_0}{2\pi}\frac{\partial\phi}{\partial t}\,, \tag{26.5.22}$$

that is, the gauge-invariant phase difference is given by

$$\Delta\phi - \frac{2\pi}{\Phi_0}\int \varphi(t')\mathrm{d}t'\,. \tag{26.5.23}$$

When the potential is denoted by V instead of φ, the previous formula is recovered.

When a finite voltage is applied, the phase difference changes with time. In particular, for a DC voltage

$$\phi_{\mathrm{R}} - \phi_{\mathrm{L}} = \delta\phi_0 + 2\frac{eV}{\hbar}t\,. \tag{26.5.24}$$

Because of the linear time dependence of the phase difference, the current through the junction oscillates sinusoidally:

$$I_{\mathrm{J}} = I_0 \sin\left(\delta\phi_0 + 2\frac{eV}{\hbar}t\right) = I_0 \sin\left(\delta\phi_0 + 2\pi\frac{V}{\Phi_0}t\right). \tag{26.5.25}$$

Thus a DC voltage gives rise to an alternating current of angular frequency $\omega = 2eV/\hbar = 2\pi V/\Phi_0$ – that is, of frequency

$$\nu = \frac{2e}{h}V\,. \tag{26.5.26}$$

This is the *alternating-current (AC) Josephson effect*, and the quantity

$$K_{\mathrm{J}} = \frac{2e}{h} = 483\,597.9\,\mathrm{GHz/V} \tag{26.5.27}$$

is called the Josephson constant. Since the above relation between the frequency and voltage is independent of the material properties, and is satisfied

to a high precision, the AC Josephson effect has been used to define the voltage standard since 1990.

The phenomenon can be interpreted as follows. In order to remain a bound pair after tunneling, the superconducting pair of electrons emits a photon of energy $\hbar\omega = 2eV$, which compensates the difference between the chemical potentials on the two sides. The phenomenon was confirmed experimentally by the detection of the radiation, which is in the microwave region when the applied voltage is a few millivolts.[18]

In the *inverse AC Josephson effect* an AC voltage (a microwave field) of frequency ω and amplitude V_ω and an additional DC voltage V_0 are applied to the Josephson junction. The total voltage that determines the difference of the chemical potentials is

$$V(t) = V_0 + V_\omega \cos \omega t \,. \tag{26.5.28}$$

Substituting this into (26.5.15), the equation governing the variation of the phases with time,

$$\frac{\partial}{\partial t}(\phi_\mathrm{R} - \phi_\mathrm{L}) = \frac{2e}{\hbar} V_0 + \frac{2e}{\hbar} V_\omega \cos \omega t \tag{26.5.29}$$

is obtained. By integrating both sides,

$$\phi_\mathrm{R} - \phi_\mathrm{L} = \delta\phi_0 + \frac{2e}{\hbar} V_0 t + \frac{2e}{\hbar} \frac{V_\omega}{\omega} \sin \omega t \,, \tag{26.5.30}$$

and the current through the junction is

$$I_\mathrm{J} = I_0 \sin \left(\delta\phi_0 + \frac{2e}{\hbar} V_0 t + \frac{2e}{\hbar} \frac{V_\omega}{\omega} \sin \omega t \right). \tag{26.5.31}$$

This formula can be cast in a more transparent form by applying a consequence of (C.1.50):

$$\begin{aligned} \cos(a \sin \omega t) &= \sum_{n=-\infty}^{\infty} J_n(a) \cos n\omega t \,, \\ \sin(a \sin \omega t) &= \sum_{n=-\infty}^{\infty} J_n(a) \sin n\omega t \,, \end{aligned} \tag{26.5.32}$$

where J_n is the Bessel function of order n. Making use of the property

$$J_{-n}(x) = (-1)^n J_n(x) \tag{26.5.33}$$

of the Bessel functions, the current through the Josephson junction is

$$I_\mathrm{J} = I_0 \sum_{n=-\infty}^{\infty} (-1)^n J_n\Big(\frac{2eV_\omega}{\hbar\omega}\Big) \sin \left[\delta\phi_0 + \left(\frac{2eV_0}{\hbar} - n\omega \right) t \right]. \tag{26.5.34}$$

[18] An applied voltage of 1 mV corresponds to a frequency of 483.6 GHz.

The total current through a junction placed in a microwave cavity is the sum of the various AC components. In the absence of an applied DC voltage ($V_0 = 0$) the term $n = 0$ gives a DC component, but the factor $J_0(2eV_\omega/\hbar\omega)$ makes the amplitude smaller than the maximum current that can be driven through the junction in the absence of the microwave field. Moreover, DC components appear at all values of V_0 that satisfy

$$V_0 = n\frac{\hbar\omega}{2e}\,. \tag{26.5.35}$$

The corresponding current–voltage characteristic is shown in Fig. 26.28(a).

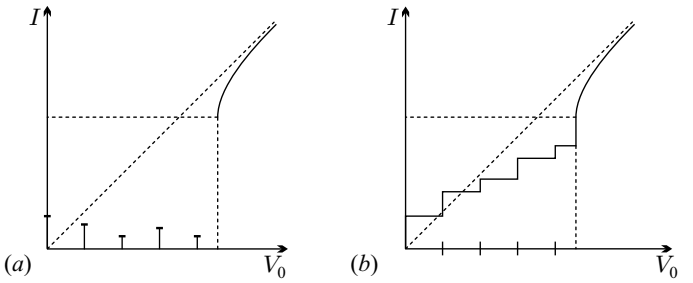

Fig. 26.28. Current–voltage characteristics for a Josephson junction in a microwave field with (a) voltage drive and (b) current drive

The situation is different when the junction is not connected to a voltage source but to a current generator, which is highly common in experiments. In this case the additional current component due to normal electrons must also be taken into account. Assuming ohmic current–voltage characteristics for this component at voltages $V > 2\Delta/e$, and adding the corresponding term to the phenomenological equations for the current, we have

$$I = I_0 \sin(\phi_\mathrm{R} - \phi_\mathrm{L}) + V/R\,, \tag{26.5.36}$$

where the phase difference and the voltage continue to be related by (26.5.21). The total current then satisfies the equation

$$I = I_0 \sin(\phi_\mathrm{R} - \phi_\mathrm{L}) + \frac{\hbar}{2eR}\frac{\partial}{\partial t}(\phi_\mathrm{R} - \phi_\mathrm{L})\,. \tag{26.5.37}$$

If this total current, rather than the voltage, is fixed externally, very different I–V curves are obtained. When the phase difference and, through it, the voltage are determined from the current, steps are found instead of discrete peaks, as shown in Fig. 26.28(b). They are called *Shapiro steps*.[19] The height of the

[19] S. Shapiro, 1963.

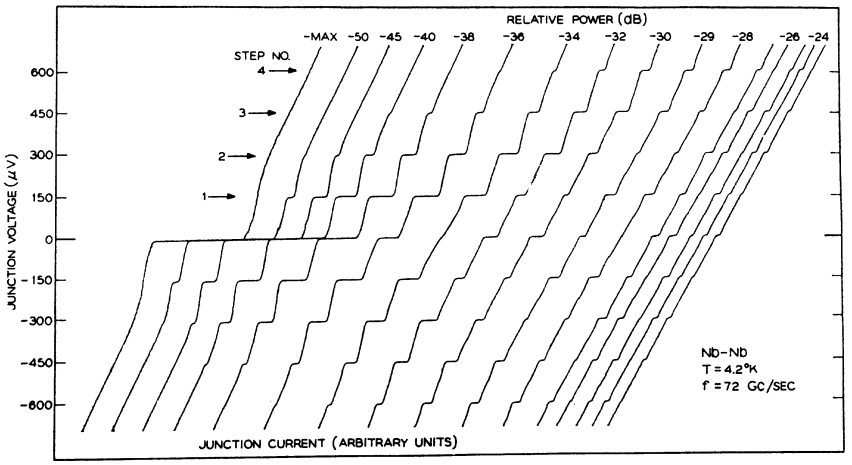

Fig. 26.29. The current–voltage characteristics for a current-driven Josephson junction placed in microwave fields of different power, according to the measurements of C. C. Grimes and S. Shapiro [Reprinted with permission from *Phys. Rev.* **169**, 397 (1968). ©1968 by the American Physical Society]

nth step is determined by the Bessel function J_n. As indicated in Fig. 26.29, measurements are in fair agreement with the theoretical description.

The situation is more complicated when coupling between the two superconductors cannot be approximated by a linear term as in (26.5.6). However, the discussion of this point would lead us too far afield.

26.5.4 Josephson Junctions in a Magnetic Field

It is known from the Ginzburg–Landau theory that the phase of the superconductor is changed by the magnetic field. It is expected to change the current through the junction, too. Consider a setup in which the sample is uniform and infinite in the y- and z-directions, and the narrow insulating oxide layer is centered at the plane $x = 0$. The magnetic field is applied in the z-direction (i.e., parallel to the surface of the oxide layer), and its strength depends on the variable x. It can be derived from an x-dependent vector potential with a nonvanishing y component, $\boldsymbol{A} = A_y(x)\hat{\boldsymbol{y}}$, which satisfies

$$B_z = \frac{\mathrm{d}A_y(x)}{\mathrm{d}x}\,. \tag{26.5.38}$$

$B_z(x)$ and $A_y(x)$ vary considerably only close to the oxide layer, in a region whose width is on the order of the penetration depth, as illustrated in Fig. 26.30.

In addition to the x-directed current through the junction, a y-directed surface current appears in the above-mentioned region. Its spatial variation is shown in Fig. 26.30.

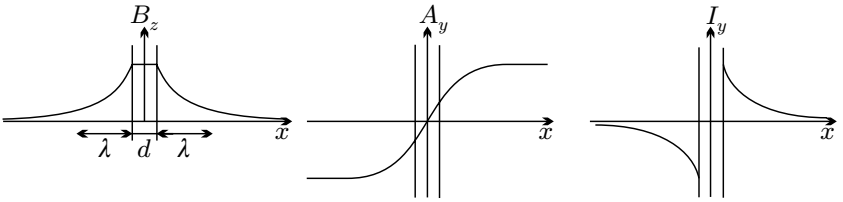

Fig. 26.30. The spatial variation of the magnetic induction, vector potential, and surface current in a Josephson junction, perpendicular to the oxide layer

Because of the presence of the vector potential, the phase of the superconductor is not homogeneous: it depends on the y coordinate. The x-directed current density at position y through the junction is determined by the phase difference $\phi(L_y) - \phi(R_y)$, where L_y and R_y are two points inside the left- and right-hand superconductors, respectively, whose distance from the interface is larger than the penetration depth. To determine this phase difference, consider the second Ginzburg–Landau equation (26.4.30). Expressed in terms of the phase of the wavefunction, the current density is

$$\boldsymbol{j} = -\frac{e^*\hbar}{m^*}|\psi|^2 \left(\boldsymbol{\nabla}\phi + \frac{e^*}{\hbar}\boldsymbol{A} \right). \tag{26.5.39}$$

Far from the insulator–superconductor interface, where no current flows,

$$\boldsymbol{\nabla}\phi = -\frac{e^*}{\hbar}\boldsymbol{A}\,. \tag{26.5.40}$$

The integral of this formula gives the phase difference between two points that can be connected by a path that is entirely in the superconductor.

Now consider two points, L_1 and L_2, deep inside the left-hand superconductor, as in Fig. 26.31.

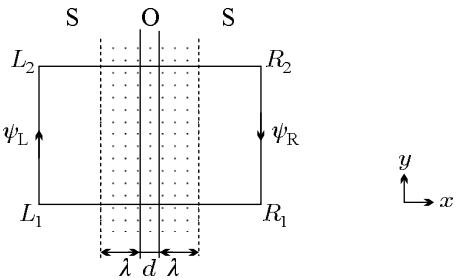

Fig. 26.31. Schematic cross section of a Josephson junction in a magnetic field that is applied in z-direction

Although the magnetic field cannot penetrate to this depth, the difference of the phases at the two points is finite because of the presence of the vector potential:

$$\phi(L_2) - \phi(L_1) = -\frac{e^*}{\hbar} \int_{L_1}^{L_2} \boldsymbol{A} \cdot \mathrm{d}\boldsymbol{l} \,. \tag{26.5.41}$$

Analogously, for two points R_1 and R_2 deep inside the right-hand side but with the same y and z coordinates as L_1 and L_2, the phase difference is

$$\phi(R_2) - \phi(R_1) = -\frac{e^*}{\hbar} \int_{R_1}^{R_2} \boldsymbol{A} \cdot \mathrm{d}\boldsymbol{l} \,. \tag{26.5.42}$$

A suitable rearrangement leads to the following expression for the variation of the phase difference between points located on opposite sides of the junction:

$$\begin{aligned} \Delta\phi(L_2 - R_2) - \Delta\phi(L_1 - R_1) &= [\phi(L_2) - \phi(R_2)] - [\phi(L_1) - \phi(R_1)] \\ &= [\phi(L_2) - \phi(L_1)] - [\phi(R_2) - \phi(R_1)] \\ &= -\frac{e^*}{\hbar} \left(\int_{L_1}^{L_2} \boldsymbol{A} \cdot \mathrm{d}\boldsymbol{l} - \int_{R_1}^{R_2} \boldsymbol{A} \cdot \mathrm{d}\boldsymbol{l} \right) . \end{aligned} \tag{26.5.43}$$

Since only the y component of the vector potential is nonzero, the line integrals along the x-directed paths between L_1 and R_1, and L_2 and R_2 vanish. Owing to their vanishing contributions, these segments can be freely added to the previous integration path, and so

$$\Delta\phi(L_2 - R_2) - \Delta\phi(L_1 - R_1) = \frac{e^*}{\hbar} \oint \boldsymbol{A} \cdot \mathrm{d}\boldsymbol{l} \,, \tag{26.5.44}$$

where the closed path is traversed counterclockwise. This can be rewritten as a surface integral for $\operatorname{curl} \boldsymbol{A}$, which gives the flux Φ through the surface bounded by the contour. In terms of the flux quantum Φ_0 we have

$$\Delta\phi(L_2 - R_2) - \Delta\phi(L_1 - R_1) = 2\pi \frac{\Phi}{\Phi_0} \,. \tag{26.5.45}$$

Denoting the phase difference at $y = 0$ by $\Delta\phi(0)$, the phase difference at an arbitrary y is given by

$$\Delta\phi(y) = \Delta\phi(0) + 2\pi \frac{\Phi(y)}{\Phi_0} \,, \tag{26.5.46}$$

where

$$\Phi(y) = B \cdot (d + \lambda_\mathrm{L} + \lambda_\mathrm{R}) y \tag{26.5.47}$$

approximately. In the previous formula d is the thickness of the oxide layer, while λ_L and λ_R are the penetration depths in the two superconductors. The Josephson current at position y is therefore

$$I_{\mathrm{J}}(y) = I_0 \sin\left(\Delta\phi(0) + 2\pi\frac{\Phi(y)}{\Phi_0}\right). \tag{26.5.48}$$

Note that this formula allows the current to be interpreted as the sine of the gauge-invariant phase difference

$$\Delta\phi + \frac{2\pi}{\Phi_0}\int \boldsymbol{A}\cdot \mathrm{d}\boldsymbol{s} \tag{26.5.49}$$

in the presence of a vector potential.

The formulas also shows that the current through the junction oscillates with the height y. This is illustrated in Fig. 26.32.

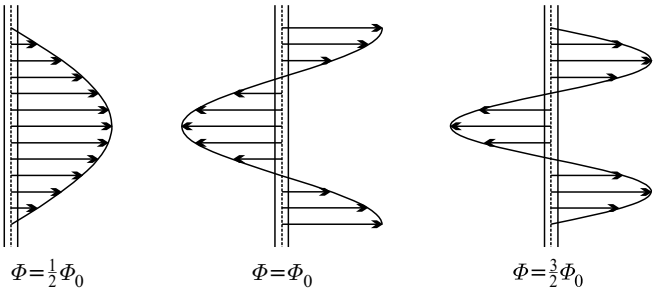

Fig. 26.32. The spatial variation of the current through the Josephson junction, perpendicular to the magnetic field, for three different values of the field strength

Because of this spatial oscillation, the total current through the junction varies with the magnetic field much like a diffraction pattern. The current is the highest in the zero-field case, since it flows in the same direction over the entire cross section of the junction then. When the field strength is such that the total magnetic flux through the junction is an integral multiple of the flux quantum, the total current is zero because the oscillatory contributions cancel out. In general, the current through the junction for a sample of width L_y is

$$\begin{aligned} I_{\mathrm{J}} &= \int_0^{L_y} I_{\mathrm{J}}(y)\,\mathrm{d}y = I_0 \int_0^{L_y} \sin\left(\delta\phi(0) - 2\pi\frac{\Phi(y)}{\Phi_0}\right)\,\mathrm{d}y \\ &= I_0 L_y \sin(\delta\phi(0))\frac{\sin(\pi\Phi/\Phi_0)}{\pi\Phi/\Phi_0}\,, \end{aligned} \tag{26.5.50}$$

and the total flux through the junction is $\Phi = B(d + \lambda_{\mathrm{L}} + \lambda_{\mathrm{R}})L_y$. Since the direction of the current is rarely measured in experiments, the dependence of the total current on the magnetic field is similar to the Fraunhofer diffraction pattern. However, when two point-like junctions are located at two opposite points of a ring, the dependence on the magnetic field is described by the

Airy function. These two functions, along with measurement data, are shown in Fig. 26.33

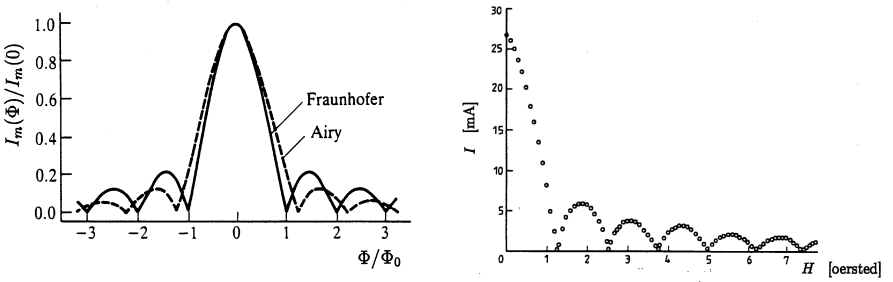

(*a*) (*b*)

Fig. 26.33. The total current through a Josephson junction as a function of the magnetic field: (*a*) theoretical predictions; (*b*) experimental results by D. E. Langenberg et al. [*Proc. IEEE* **54**, 560 (1966)]

A more interesting interference pattern is obtained when the current is split between two arms, which are connected in parallel and enclose a finite magnetic flux.

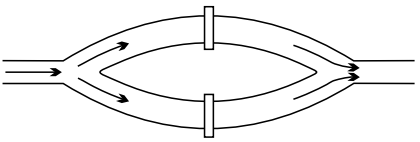

Fig. 26.34. Two Josephson junctions connected in parallel

Since the superconducting arms are broken by the insulating layers of the junction, the quantization condition does not apply to the enclosed flux: it can take any arbitrary value. Assuming that the arms are sufficiently narrow for that each junction can be characterized by a phase difference, the resultant of the currents in the two arms is

$$I_{\mathrm{J}} = I_0 \left[\sin \Delta\phi(L_1 - R_1) + \sin \Delta\phi(L_2 - R_2)\right] . \tag{26.5.51}$$

In perfect analogy with the previous results, when the two arms enclose a flux Φ, the phase differences are related by

$$\Delta\phi(L_2 - R_2) - \Delta\phi(L_1 - R_1) = 2\pi \frac{\Phi}{\Phi_0} . \tag{26.5.52}$$

Choosing the phase differences in the two arms as $\Delta\phi_0 + \pi\Phi/\Phi_0$ and $\Delta\phi_0 - \pi\Phi/\Phi_0$, the resultant current is

$$I_{\mathrm{J}} = I_0 \left[\sin\left(\Delta\phi_0 + \pi \frac{\Phi}{\Phi_0} \right) + \sin\left(\Delta\phi_0 - \pi \frac{\Phi}{\Phi_0} \right) \right] = 2 I_0 \sin \Delta\phi_0 \cdot \cos\left(\pi \frac{\Phi}{\Phi_0} \right) . \tag{26.5.53}$$

Once again, by measuring the intensity of the current but not its direction, a diffraction-pattern-like dependence is found (Fig. 26.35). The operation of SQUIDs,[20] designed to measure tiny magnetic fields,[21] is based on this principle.

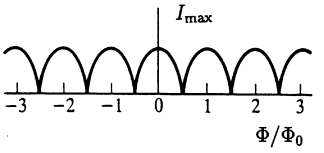

Fig. 26.35. The dependence of the maximum supercurrent on the magnetic field for two point-like Josephson junctions connected in parallel

In reality, the finite size of the Josephson junctions connected in parallel must also be taken into account. If the flux through the cross section of the junction is Φ_f then, according to (26.5.50), the previous formula for the current has to be multiplied by the appropriate factor

$$\sin\left(\pi\Phi_f/\Phi_0\right) / \left(\pi\Phi_f/\Phi_0\right), \tag{26.5.54}$$

at each junction. This leads to a much slower variation than the total enclosed flux Φ, and so the dependence shown in Fig. 26.36 is observed in experiments.

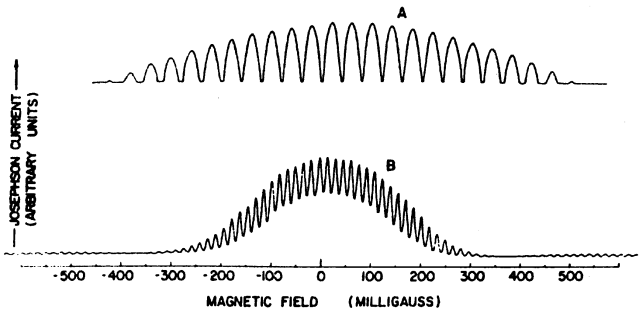

Fig. 26.36. Macroscopic interference and diffraction effects in the maximum Josephson current through two Josephson junctions coupled in parallel [Reprinted with permission from R. C. Jaklevic et al., *Phys. Rev.* **140**, A 1628 (1965). ©1965 by the American Physical Society]

[20] The acronym SQUID stands for Superconducting QUantum Interference Device.
[21] In an appropriate design, SQUIDs can also be used for the highly sensitive measurement of susceptibility and voltage.

Further Reading

1. W. Buckel and R. Kleiner, *Superconductivity: Fundamentals and Applications*, Second, Revised and Enlarged Edition, John Wiley & Sons, Ltd., New York (2004).
2. P. G. de Gennes *Superconductivity of Metals and Alloys*, W. A. Benjamin, New York (1966).
3. *Handbook of Superconductivity*, Edited by C. P. Poole, Jr., Academic Press, San Diego (2000).
4. J. B. Ketterson and S. N. Song, *Superconductivity*, Cambridge University Press, Cambridge (1999).
5. L.-P. Lévy, *Magnetism and Superconductivity*, Texts and Monographs in Physics, Springer-Verlag, Berlin (2000).
6. C. P. Poole, Jr., H. A. Farach, and R. J. Creswick, *Superconductivity*, Academic Press, San Diego (1995).
7. *Superconductivity*, Edited by R. D. Parks, Marcel Dekker, Inc., New York (1969).
8. D. R. Tilley and J. Tilley, *Superfluidity and Superconductivity*, Adam Hilger Ltd., Bristol (1986).
9. M. Tinkham, *Introduction to Superconductivity*, Second Edition, McGraw-Hill, Inc., New York (1996).